Rhythmic neuronal synchronization in visual cortex entails spatial phase relation diversity that is modulated by stimulation and attention

Published in final edited form as:
Neuroimage. 2013 July 1; 74: 99–116. doi:10.1016/j.neuroimage.2013.02.007.

Rhythmic neuronal synchronization in visual cortex entails spatial phase relation diversity that is modulated by stimulation and attention

Eric Maris[1], **Thilo Womelsdorf**[1,2], **Robert Desimone**[3,4], and **Pascal Fries**[1,5]

[1]Donders Centre for Brain, Cognition, and Behaviour, Radboud University Nijmegen, 6525 EN Nijmegen, The Netherlands. [2]Department of Biology, Faculty of Science and Engineering, York University, Toronto, Ontario, M3J 1P3. [3]Laboratory of Neuropsychology, National Institute of Mental Health, National Institutes of Health, Bethesda, MD 20892, USA. [4]McGovern Institute for Brain Research at MIT, Cambridge, MA 02139, USA. [5]Ernst Strüngmann Institute (ESI) for Neuroscience in Cooperation with Max Planck Society, 60528 Frankfurt am Main, Germany.

Abstract

Groups of neurons tend to synchronize in distinct frequency bands. Within a given frequency band, synchronization is defined as the consistency of phase relations between site pairs, over time. This synchronization has been investigated in numerous studies and has been found to be modulated by sensory stimulation or cognitive conditions. Here, we investigate local field potentials (LFPs) and multi-unit activity (MUA) recorded from area V4 of two monkeys performing a selective visual attention task. We show that phase relations, that are consistent over time, are typically diverse across site pairs. That is, across site pairs, mean phase relations differ substantially and this across-site-pair phase-relation diversity (SPHARED, for Spatial PHAse RElation Diversity) is highly reliable. Furthermore, we show that visual stimulation and selective attention can shift the pattern of phase relations across site pairs. These shifts are again diverse and this across-site-pair phase-relation-shift diversity (SPHARESD) is again highly reliable. We find SPHARED for LFP-LFP, LFP-MUA and MUA-MUA pairs, stimulus-induced SPHARESD for LFP-LFP and LFP-MUA pairs, and attention-induced SPHARESD for LFP-LFP pairs. SPHARESD is a highly interesting signal from the perspective of impact on downstream neuronal activity. We provide several pieces of evidence for such a role.

Keywords

Phase; Synchronization; Oscillation; Gamma; Alpha; Theta; Attention; Selection; Monkey; Visual

Introduction

Neuronal synchronization occurs in distinct frequency bands, as is clear from the oscillations that are often observed in local field potentials (LFPs). The amplitude of these oscillations is

Corresponding author: Eric Maris, Tel.: +31-243612651, Fax.: +31-243616066, e.maris@donders.ru.nl.

related to external stimuli as well as to cognitive functions such as selective attention (Womelsdorf and Fries, 2007), working memory (Pesaran et al., 2002), and sensory-motor coordination (Murthy and Fetz, 1992). Oscillatory amplitude measures the degree of local synchronization of neuronal activity, which is an important parameter of the putative mechanisms that underlie cognitive functions (Engel et al., 2001; Buzsaki and Draguhn, 2004; Fries, 2005; Schroeder and Lakatos, 2009).

Although synchronization is likely to be relevant for the function of neuronal networks, extended synchronization across neuronal space prohibits flexibility and differentiation in information processing. Therefore, functional synchronization likely involves oscillations that are coherent, but rather than being zero-phase-synchronous across space, they might have systematic phase differences or phase relations. From the perspective of cognitive functions, phase relation is a highly interesting neuronal variable because it can vary on a much faster timescale than the comparatively slow amplitude fluctuations. Therefore, phase relations could reflect fast neuronal mechanisms that underlie cognitive functions.

We investigated phase relations across multiple sites in awake macaque area V4 while the animals were engaged in a perceptual task involving attentional selection. We found diversity in these phase relations in three discrete frequency bands: theta, alpha and gamma. We also found that the presentation of a visual stimulus produced substantial and reliable shifts in these phase relations, in exactly the same three frequency bands.

Materials and Methods

Experimental Procedure

Experiments were performed in two hemispheres of two male rhesus monkeys (macaca mulatta), and followed guidelines of the National Institutes of Health with approval by the National Institute of Mental Health Intramural Animal Care and Use Committee. Experimental procedures for data collection have been described in detail elsewhere (Fries et al., 2001; Fries et al., 2008) and are summarized below. We localized the prelunate gyrus using MRI scans. Recording chambers were then implanted over the prelunate gyrus under surgical anesthesia. Small trepanations of the skull were performed within the recording chamber. Through the trepanation, four tungsten microelectrodes (impedances of 1–2 MΩ) were advanced separately at a very slow rate (1.5 μm/s) to minimize deformation of the cortical surface by the electrode (“dimpling”). Electrodes tips were separated by 650 or 900 μm. Data amplification, filtering and acquisition were done with a Multichannel Acquisition Processor (Plexon Inc.). The signal from each electrode was passed through a headstage with unit gain and then split to separately extract the spike and the LFP components. For spike recordings, the signals were filtered with a passband of 100–8000 Hz, further amplified and digitized at 40 kHz. A threshold was set interactively and spike waveforms were stored for a time window from 150 μs before to 700 μs after threshold crossing. The threshold clearly separated spikes from noise, but was chosen to include multi-unit activity. Offline, we performed a principal component analysis of the waveforms and plotted the first against the second principal component. Those waveforms that corresponded to artifacts were excluded. For multi-unit analyses, all other waveforms were accepted and the times of threshold crossing were kept and down-sampled to 1 kHz. For LFP recordings, the signals were filtered with a passband of 0.7–170 Hz, further amplified and digitized at 1 kHz.

The analyses in this study crucially depend on the phase relations between LFP and MUA channels. For this reason it is important that our phase relation estimates can be trusted and do not depend on confounding factors such as electrode impedance. For our headstage model, electrode type and impedance, the absolute phase shift is less than two degrees, and

the resulting non-physiological between-electrode phase relations would be much smaller than that (Chris Heydrick, Plexon Inc., personal communication, May 22, 2012).

At the start of the recordings, each electrode was lowered separately until it recorded visually driven activity. Once this had been achieved for all electrodes, we fine tuned the electrode positions to optimize the signal-to-noise ratio of the multiple spike recordings and to obtain as many isolated single units as possible. Since the penetration was halted as soon as clear visually driven activity was obtained, most of the recordings were presumably done from the superficial layers of the cortex. To confirm the recording position without sacrificing the animal, we obtained a structural magnetic resonance image (MRI) with one electrode in place, confirming the placement in the appropriate portion of the prelunate gyrus. Receptive field (RF) position and neuronal stimulus selectivity were as expected for the target part of area V4.

Visual stimulation and experimental paradigm

Stimuli were presented on a 17 inch CRT monitor 0.57 m from the monkey's eyes that had a resolution of 800*600 pixel and a screen refresh rate of 120 Hz non-interlaced. Stimulus generation and behavioral control were accomplished with the CORTEX software package (www.cortex.salk.edu).

A trial started when the monkey touched a bar and directed its gaze within 0.7° of the fixation spot on the computer screen. When we used trial-by-trial cueing of selective attention, first the cue appeared, followed after 1500–2000 ms by a pair of stimuli of which one was cued (see below for more details on the different cueing regimes used). Both stimuli were patches of drifting square wave luminance gratings with a frequency between 0.8333 and 1.8750 Hz (one out of five possible frequencies), differing across sessions. One of the two patches was presented inside the RF of the recorded neuronal population, and the other was presented outside this RF. Procedures for the initial mapping of visual RFs and orientation tuning have been described elsewhere (Fries et al., 2008). For the present study, it is important to know that the RFs of the multiple recording sites typically overlapped substantially. For the recordings, we selected a stimulus orientation that had resulted in a strong co-activation of the simultaneously recorded units. Note that the selected grating could therefore not activate all sites to the same extent, but necessarily ended up being suboptimal or (rarely) even suppressive for some sites. The second patch of drifting grating that was placed outside the RF was identical to the inside-RF patch with regard to eccentricity, size, contrast, spatial and temporal frequency, but its orientation was rotated by 90°. This was done in order to avoid pre-attentive perceptual binding of the two patches of grating. Two patches of grating moving in orthogonal direction can nevertheless be perceived as part of one pattern moving behind two apertures, if the movement directions are consistent with this interpretation. To preclude this, the movement direction of the patch outside the RFs was chosen to be inconsistent with this interpretation. For most recording sessions, the orientation of the outside-RF patch was 90° away (counterclockwise) from the inside-RF patch at that eccentricity. For a subset of recordings, it was moved to be as close as possible to the RF without evoking a stimulus driven response.

The general task of the monkey was to release the bar between 150 and 650 ms after a change in color of the cued stimulus. The color change occurred at an unpredictable moment in time between 500 and 5000 ms after stimulus onset, with change times drawn from a normal probability distribution. Successful trial completion was rewarded with four drops of diluted apple juice. If the monkey released the bar too early or if it moved its gaze out of the fixation window, the trial was immediately aborted and followed by a timeout.

Both stimuli could change color with equal likelihood, and their change time distributions were equal. The monkey's task was to respond to color changes in the stimulus that was cued (using one of three cueing paradigms; see below) as target and ignore changes in the other stimulus, the distracter. The color changes were close to the monkey's detection threshold, ensuring that the task could only be performed when attention was actually allocated to the target. On the 50% of the trials in which the distracter changed color before the target, the target changed color later on in the trial. Those target changes were distributed uniformly in the remaining time between distracter changes and 5000 ms after stimulus onset. Signals recorded after the target or distracter change were not analyzed (see Trial selection and preprocessing). However, the monkey's behavioral responses on trials in which the distracter changed first inform us about their attentional engagement: correct responses (bar release within 0.15–0.65 s after target change) were made in 85% of these trials.

We used three different cueing paradigms for directing selective visual attention and all of them gave essentially identical results. Two of the paradigms used trial-by-trial cueing. The cue stayed on during the trial and was either a short line next to the fixation spot, pointing to the location of the target, or alternatively, the fixation spot color, red cueing the upper, and green cueing the lower stimulus. In the rest of the recording sessions, we used a blocked trial design. Blocks consisted of 20 trials. The first two trials in a block were instruction trials in which only one of the two stimuli was shown and the monkey performed the task on that stimulus. The location of that stimulus was the target location for that block. For the remainder of the block, both stimuli were shown together without any further cue. Thus, in the block design, the different attention conditions were physically identical. We recorded 100 to 300 correctly performed trials per attention condition.

Trial selection and preprocessing

We calculated power and coherence spectra (see below for details of spectral estimation) separately for the *pre-stimulus* period (the 1500–2000 ms before stimulus onset) and for the *sustained* epoch. We defined the sustained epoch as the epoch from 300 ms after stimulus onset until the first change in one of the two stimuli. Because we wanted to compare the pre-stimulus and the sustained epochs, we also wanted to prevent any bias for the spectral estimates that could potentially be introduced by unequal lengths of the pre-stimulus and the sustained epochs. To achieve this, we equalized the lengths of these two epochs on a trial-by-trial basis. That is, for each trial, we determined whether the baseline or the sustained epoch was the shortest. The longer epoch was then shortened to the length of the shorter one by removing a segment at the beginning of the longer epoch. The resulting epochs were between 100 and 2000 ms long, but the vast majority was around 1600 ms, the modal length of the pre-stimulus period.

Our design included two attention conditions with attention directed either inside or outside the receptive field of the recorded neuronal population. These two attention conditions were compared, separately for the pre-stimulus and the sustained period. Each session had an equal number of trials in the two attention conditions.

The LFP contained two signal components that are irrelevant to the present study and that were therefore removed: (1) the power line artifact, oscillating at 60 Hz, and (2) the rhythmic signal component produced by the visual stimulation, which involves drifting square wave luminance gratings (see Visual stimulation and experimental paradigm, above). The power line artifact was removed by means of a filter based on the Discrete Fourier Transform (DFT). We first data-padded the time epochs of interest by 1.5 seconds both at the beginning (pre-padding) and the end (post-padding). We then regressed these padded epochs onto six regressors: sine and cosine functions of 60, 120, and 180 Hz, covering the

whole padded epoch. The power line artifact was effectively removed by calculating the residual of this multiple regression. The power spectra of the cleaned epochs showed a notch of a bin width of about 0.2 Hz. Finally, the pre- and the post-padding segments were removed. The actual spectral analysis used the multitaper method (see further), with a spectral smoothing beyond ±1 Hz (see below), so that the notch became invisible.

As a way to remove the rhythmic signal component produced by the visual stimulation, we subtracted the stimulus-locked average of the epoch. We did this for the sustained epochs, during which the moving grating was presented, but also for the pre-stimulus epochs, because we wanted the preprocessing to be equal for the two sets of epochs. We are aware of the fact that, due to trial-to-trial variability, subtracting the stimulus-locked average may not fully remove stimulus-evoked activity (Wang and Ding, 2011). Importantly, the effects we observed (see Results) were all in frequency bands well above the visual stimulation frequency.

Spectral analysis

We performed spectral analysis using multi-tapers to achieve optimal spectral concentration (Mitra and Pesaran, 1999; Jarvis and Mitra, 2001; Pesaran et al., 2002). Multitaper methods involve the use of multiple data tapers for spectral estimation. A segment of data is multiplied by a data taper before taking the Fourier transform. A variety of tapers can be used, but an optimal family of orthogonal tapers is given by the prolate spheroidal functions or Slepian functions. These are parameterized by their length in time, T, and their bandwidth in frequency, W. For a choice of T and W, up to K=2TW-1 tapers are concentrated in frequency and suitable for use in spectral estimation. The bandwidth parameter W corresponds to a spectral smoothing window [f−W,f+W] Hz, centered at frequency f. Exploratory data analysis demonstrated several discrete rhythms , namely a theta (3–4 Hz), an alpha (9–13 Hz) and a gamma (35–75 Hz) frequency rhythm. The corresponding frequency bands varied in width, with the width increasing with the main frequency of the component. For this reason, we used different spectral smoothing, as determined by W, for the low and the high frequencies. For the frequencies from 2 to 22 Hz, we used W=1, and for the frequencies from 22.5 to 120 Hz, we used W=14.

In multitaper estimation, for each taper, the data segment is multiplied with that taper and then Fourier transformed, giving the windowed Fourier transform, $\tilde{x}_k(f)$:

$$\tilde{\mathrm{x}}_{\mathrm{k}}(\mathrm{f})=\sum_{t=1}^{N} w_k(t)\,x_t\,e^{-2\pi i f t}$$

where x_t, ($t = 1,2, \ldots, N$) is the time series of the signal under consideration and $w_k(t)$, ($k = 1,2, \ldots, K$) are K orthogonal taper functions. For spike signals, the firing rate was represented as a binary process with a bin width of one millisecond, and then subjected to spectral analysis like LFPs. The mean of the epoch was subtracted before Fourier transformation, both for LFP and spike signals.

The multitaper estimates for the spectrum $S_x(f)$ and the cross-spectrum $S_{xy}(f)$ are given by

$$S_x(f)=\frac{1}{K}\sum_{k=1}^{K}\left|\tilde{x}_k(f)\right|^2$$

$$S_{xy}(f)=\frac{1}{K}\sum_{k=1}^{K}\tilde{x}_k(f)\tilde{y}_k^*(f)$$

Spectra and cross-spectra are averaged over trials before calculating the coherency $C_{xy}(f)$

$$C_{xy}(f)=\frac{S_{xy}(f)}{\sqrt{S_x(f)S_y(f)}}$$

Coherency is a complex quantity. Its absolute value $|C_{xy}(f)|$ is termed coherence and ranges from 0 to 1. A coherence value of 1 indicates that the two signals have a constant phase relationship (and amplitude covariation), a value of 0 indicates the absence of any phase relationship. The phase of coherency is the preferred (i.e. average) phase relation between the two time series, x_t and y_t.

Within the experimental conditions of our experiment, different epochs have unequal lengths. Because the spectral resolution of the Fourier transform depends on the epoch length, and the epoch-specific spectra must be averaged over epochs, the tapered data segments were padded with zeros to a length of 2 seconds. By means of this zero-padding, we obtained an identical spectral resolution of 0.5 Hz for all epoch-specific spectra. This zero-padding had a negligible effect on the phase relation estimates, on which most of our data analysis is based (see Split-half reliability analysis of the phase relations). Following up on a comment by one of the reviewers, we also analyzed our data using a fixed data segment length of 1.5 s. (82% of our data segments were larger than 1.5 s) and found that, for most of the figures, one had to look closely to see the differences between the two analyses (zero-padded to 2 s and non-padded fixed 1.5 s.). Because of this negligible difference and because the padding allowed us to use 18% more data segments, we decided to report on the original analysis.

Across sessions, we obtained recordings from 70 sites, and simultaneous recordings from 102 site pairs. Six site pairs were removed from the analyses, because we could not estimate their LFP-MUA coherency as a result of a very low number of spikes. Our analyses were based on the signals obtained from the remaining 96 site pairs, from which we obtained 192 ordered LFP-LFP channel pairs and 192 corresponding LFP-MUA channel pairs. Please note that each unordered LFP-LFP channel pair {A,B} appeared twice in the analyses: once in the order (A,B) and once in the reverse order (B,A). This was done to be able to investigate the relation between, on the one hand, the LFP-LFP channel pairs and, on the other hand, the corresponding LFP-MUA channel pairs. Statistical testing (described in detail below) will account for this.

Split-half reliability analysis of the phase relations

Investigating phase relations across site pairs requires that these phase relations can be reliably estimated. Importantly, this reliability is *across trials*, and this must be contrasted with the possible diversity in the phase relations, which is *across site pairs*. We evaluated the reliability of the phase relations both for the LFP-LFP and LFP-MUA channel pairs, and we did this by means of a split-half reliability analysis. This analysis starts by partitioning the trials into two halves, and calculating the phase relations for each of the two halves separately. This produces two estimates of each phase relation, one for each partition. We partitioned the trials both randomly and based on whether their rank number in the session was odd or even. Both ways of partitioning gave essentially the same results and therefore

we only report the results of the odd-even split. We provide visual information about the reliability of the phase relations by plotting the phase relations for the two halves in a scatter plot (e.g., Fig. 2). In this scatter plot, we show the phase relations for all ordered channel pairs, that is, both in the order (A,B) and in the reverse order (B,A) (with A and B denoting channels). The points in the scatter plots were color-coded according to the coherence of the corresponding channel pair.

Across-site-pair phase relation diversity (SPHARED) spectra

We calculated spectra that provide information about the diversity of the phase relations over the $P = 192$ site pairs. We calculated an index of phase relation diversity based on the split-half reliability analysis. For each site pair p, we obtained the complex coherency $C_p(f)$ for the complete set of trials, and the complex coherencies $C_{p1}(f)$ and $C_{p2}(f)$ for the two partitions of trials. In the following, we will suppress the dependence on frequency and write C_p instead of $C_p(f)$. It is convenient to express the coherency C_p in polar coordinates: $A_p\exp(i\phi_p)$, in which $A_p=|C_p|$, the coherence, and ϕ_p is the phase relation. Similarly, for the two partition-specific coherencies: $C_{p1} = A_{p1}\exp(i\phi_{p1})$ and $C_{p2} = A_{p2}\exp(i\phi_{p2})$.

Our SPHARED index is based on a linear transform of the two partition-specific phase relations ϕ_{p1} and ϕ_{p2}:

$$\bar{\phi}_p=(\phi_{p1}+\phi_{p2})/2$$

$$\check{\phi}_p=(\phi_{p1}-\phi_{p2})/2$$

These linear combinations are the coordinates of the vector (ϕ_{p1}, ϕ_{p2}) in a new basis spanned by the vectors (1,1) and (1,−1) (see Fig. 1). The logic behind this linear transform is that $\bar{\phi}_p$ reflects the common component in (ϕ_{p1}, ϕ_{p2}), and $\check{\phi}_p$ reflects the component on which the elements ϕ_{p1} and ϕ_{p2} differ. If phase diversity is random, then the points in the split-half scatter plot distribute roughly within a circle and the variability in the $\bar{\phi}_p$-coordinates is approximately equal to the variability in the $\check{\phi}_p$-coordinates. The variability in the $\bar{\phi}_p$ - and the $\check{\phi}_p$-coordinates is quantified by the magnitudes of the circular means $(1/P)\sum_{p=1}^{P}A_p\exp(i\bar{\phi}_p)$ and $(1/P)\sum_{p=1}^{P}A_p\exp(i\check{\phi}_p)$. The larger the variability in either the $\bar{\phi}_p$- or the $\check{\phi}_p$-coordinates, the *smaller* the corresponding circular means. The SPHARED index is the difference between the magnitudes of the two circular means:

$$\text{SPHARED}=\left|\frac{\sum_{p=1}^{P}A_p\exp(i\check{\phi}_p)}{P}\right|-\left|\frac{\sum_{p=1}^{P}A_p\exp(i\bar{\phi}_p)}{P}\right| \quad (1)$$

SPHARED increases with the variability in the $\bar{\phi}_p$-coordinates and decreases with the variability in the $\check{\phi}_p$-coordinates. Note that the variability is defined relative to the phases of the circular means $(1/P)\sum_{p=1}^{P}A_p\exp(i\bar{\phi}_p)$ and $(1/P)\sum_{p=1}^{P}A_p\exp(i\check{\phi}_p)$, which are weighted by the coherences A_p; the more similar the phase relations $\bar{\phi}_p$ and $\check{\phi}_p$ ($p = 1, \ldots, P$) to the phases of these circular means, the larger the magnitude of the corresponding circular mean.

Because SPHARED is calculated using the circular means of the quantities $A_p\exp(i\bar{\phi}_p)$ and $A_p\exp(i\check{\phi}_p)$, which both depend on the coherences A_p, also SPHARED depends on these coherences. As a result of this weighting by coherence, the phase relation diversity in the

high-coherent channel pairs have a stronger impact on the SPHARED index than the phase relation diversity in the low-coherent channel pairs. Importantly, there is only a dependence on coherence if there is reliable (i.e., non-random) diversity in the phase relations. Otherwise, the variability in the $\bar{\phi}_p$-coordinates is equal to the variability in the $\check{\phi}_p$-coordinates, and the two terms on the right-hand side of (1) are equal, which means that the phase diversity is random.

We also analyzed our data using alternative SPHARED indices that do not depend on coherence. With these alternative SPHARED indices we obtained very similar results, but these were less reliable. In one alternative SPHARED index, the numerators on the right-hand side of (1) were replaced by the unweighted sums $\sum_{p=1}^{P}\exp(i\bar{\phi}_p)$ and $\sum_{p=1}^{P}\exp(i\check{\phi}_p)$. This alternative index has the disadvantage that the phase relations of coherent and incoherent channel pairs are weighted equally. As a result, these unweighted SPHARED indices were less reliable and their spectral structure was less clear than the structure of the original coherence-weighted SPHARED indices. This was most clearly the case for SPHARED indices that were calculated on LFP-MUA phase relations, which are less reliable than the LFP-LFP phase relations.

In a second alternative SPHARED index, we normalized for coherence: instead of dividing the terms $\sum_{p=1}^{P}A_p\exp(i\bar{\phi}_p)$ and $\sum_{p=1}^{P}A_p\exp(i\check{\phi}_p)$ by P (see Eq. 1), in this normalized SPHARED index they are divided by the summed coherence $\sum_{p=1}^{P}A_p$. The spectral structure of these normalized SPHARED indices was less clear than the structure of the original SPHARED indices. This is because, in several analyses (in particular, those involving MUA channels), some coherences are close to zero. Because these near-zero coherences also contain estimation error, the result of the normalization (which involves division by these near-zero coherence values) is very unreliable.

With a single exception (Fig. 3*A*), we will only show coherence-weighted SPHARED spectra without normalization, because these are more reliable. We will *not* compare these coherence-weighted SPHARED spectra between experimental conditions. We mention this because both coherence and SPHARED depend (however, in different ways) on the number of trials, the signal power (for the LFP channels), and the firing rate (for the MUA channels), and these quantities may differ between the experimental conditions. Coherence increases with signal power and firing rate, and decreases with the number trials (although this effect is very small when the number of trials exceeds 100). SPHARED increases with all three quantities because they all increase the reliability of the phase relation estimates ϕ_{p1} and ϕ_{p2}.

For the interpretation of the SPHARED spectra, two aspects are crucial. First, systematic across-site-pair phase relation diversity will always be reflected in a non-zero SPHARED index, regardless of weighting by or normalizing for coherence. Second, random across-site-pair phase relation diversity will always be reflected in a zero SPHARED index, regardless of weighting or normalization.

Centering the LFP-MUA phase relations

LFP-LFP phase relations clustered around zero. Therefore, the clouds of points in the split-half scatter plots were nicely centered around the point (0,0). This was not the case for the LFP-MUA phase relations, which were clustered around $4\pi/5$, which corresponds to a preferred spiking phase just before the trough of the LFP. As a result, many of the LFP-MUA phase relations were close to the discontinuity at $-\pi/+\pi$. This produced split-half

scatter plots with clusters of points in all four corners of the plot, instead of only in the center. Therefore, to more orderly display the LFP-MUA phase relations in a scatter plot, they were shifted by their average phase relation, calculated over all LFP-MUA pairs. This average phase relation was calculated as follows:

$$\mathrm{Arg}\left(\sum_{p=1}^{P} A_p \exp(i\phi_p)\right),$$

in which the Arg-operator returns the angle of a complex number. As a result of this centering operation, the cloud of points in the scatter plot was centered around the point (0,0).

Centering was also performed in the calculation of the *LFP-centered* LFP-MUA phase relations, but for a different reason. The motivation for LFP-centering was that diversity in the LFP-MUA phase relations is partly due to diversity across LFP channels for a fixed MUA channel. We wanted to quantify the diversity in the LFP-MUA phase relations in a way that did not reflect this latter source of diversity. We did this by quantifying the diversity in the LFP-MUA phase relations *within* an LFP signal. For each LFP signal, we centered at zero the three LFP-MUA phase relations involving this LFP signal, resulting in the so-called *LFP-centered* LFP-MUA phase relations. In fact, the LFP-MUA phase relations were shifted by the average phase relation, calculated over all LFP-MUA channel pairs that involve the same LFP channel. Let this set of LFP-MUA channel pairs be denoted by $\mathscr{S}$ Then, the average phase relation for this set was calculated as follows:

$$\mathrm{Arg}\left(\sum_{p \mathrm{in} \mathscr{S}} A_p \exp(i\phi_p)\right)$$

The LFP-centered LFP-MUA phase relations were obtained by subtracting this LFP-channel-specific average from the original LFP-MUA phase relations.

Split-half reliability analysis of the stimulus- and the attention-induced phase relation shifts and SPHARESD spectra

To investigate the role of the phase relations in neuronal information processing, we investigated whether there are reliable stimulus- and attention-induced phase relation shifts. We first describe how this was done for the stimulus-induced phase relation shifts. The basis of our calculations are trial-specific estimates of stimulus-induced phase relation shifts. Each trial has a pre-stimulus and a sustained stimulation epoch, and we calculated the phase relations for each period separately. We then calculated the trial-specific sustained-minus-pre-stimulus phase relation shifts ϕ_{pj}, in which p indexes the site pairs and j indexes the trials ($j = 1, \ldots, J$, with J being the total number of trials). We then represented these phase shifts on the unit-radius complex circle by calculating the complex numbers $\exp(i\phi_{pj})$. Next, we calculated the trial-average of these complex-valued phase shifts:

$$C_p = \frac{\sum_{j=1}^{J} \exp(i\phi_{pj})}{J}$$

This C_p is a complex number of which the magnitude is a phase-locking factor (PLF, Lachaux et al., 1999) that measures the over-trials consistency in the stimulus-induced phase relation shifts, and the phase angle measures the preferred (average) phase relation shift.

This complex number corresponds to the coherency-measure that was used in our reliability analysis of the phases, and therefore we also denote it by C_p. In polar coordinates, $C_p = A_p \exp(i\phi_p)$, with $A_p = |C_p|$, the PLF, and ϕ_p preferred phase relation shift. (Instead of calculating within-trial phase relation shifts, we also calculated between-trial phase relation shifts by contrasting pre-stimulus and sustained stimulation periods coming from different trials, and obtained almost identical results as with the within-trial phase relation shifts. This observation is relevant when comparing the stimulus- and the attention-induced phase relation shifts, because the latter were calculated as *between*-trial shifts; see further.)

Our analyses of the stimulus-induced phase relation shifts were based on 168 ordered LFP-LFP channel pairs and 168 corresponding LFP-MUA channel pairs, which is less than the 192 channel pairs that were used to study the phase relations within each of the four conditions of the experiment (see further). Twenty four channel pairs were removed from our analyses, because our calculation of the PLFs of the LFP-MUA phase relation shifts required trial-specific estimates of the sustained-minus-pre-stimulus phase shifts ϕ_{pj} for *all* trials *j*. For some channels with a low number of spikes, this could not be achieved.

We evaluated the reliability of the stimulus-induced phase relation shifts using the same tools that we used to evaluate the reliability of the phase relations: split-half scatter plots and spectra of across-site-pair (spatial) phase relation *shift* diversity (SPHARESD).

Investigating phase relation shifts with attention (inside vs. outside of the receptive fields) was performed analogous to the investigation of stimulus-induced phase relation shifts. We started our calculations by grouping the trials in pairs such that each pair contained one trial in which attention was directed inside the receptive field, and another trial in which it was directed outside the receptive field. Then, for each pair of trials, we calculated the attention-induced phase relation shift, separately for the pre-stimulus and the sustained stimulation period. In the same way as for the stimulus-induced phase relation shifts, we then calculated the trial-pair-specific inside-minus-outside phase relation shifts, represented these phase relation shifts on the unit-radius complex circle, and calculated the trial-average of these complex-valued phase relation shifts. This produces a complex number of which the magnitude is a PLF that measures the over-trials consistency in the attention-induced phase relation shifts, and the phase angle measures the preferred phase relation shift. The rest of the analysis is the same as for the stimulus-induced phase relation shifts. Our analyses of the attention-induced phase relation shifts were based on the same channel pairs that were used in the analysis of the stimulus-induced phase relation shifts.

Determining statistical significance of the SPHARED and the SPHARESD spectra

SPHARED and SPHARESD spectra quantify reliable diversity in the phase relations and their stimulus- and attention-induced shifts, respectively. However, these spectra are themselves estimates and therefore have some degree of unreliability. For each frequency is it of interest to statistically test the null hypothesis that a SPHARED or SPHARSED index is equal to zero. For this statistical test, we make use of the fact that a SPHARED (SPHARESD) index is zero if the Pearson correlation between the two sets of partition-specific phase relation (shift) estimates is zero. We calculated these split-half correlations separately for each of the frequencies, and obtained one-sided p-values by transforming these correlations to Student (T) distributed random variables with $P - 2$ degrees of freedom. (We calculated one-sided p-values, because we only need sensitivity for the alternative hypothesis that the population SPHARED (SPHARESD) index is *larger* than zero.) To prevent a possible symmetry-induced bias, split-half correlations and their corresponding p-values were calculated using unique (unordered) site pairs. That is, each site pair contributed only a single pair of phase relation (shift) estimates, instead of the two pairs that were used

to construct the split-half scatter plots (corresponding to the two possible orders of a site pair).

We dealt with the multiple comparison problem (293 frequency-specific p-values) by controlling the false discovery rate (FDR, Benjamini and Hochberg, 1995; Genovese et al., 2002, see Materials and Methods) at 0.05. This was achieved by sorting the 293 p-values in ascending order and comparing them with the series [1,2, …, P] × 0.05/P (P = 293). Controlling the FDR at 0.05 implies that, among the significant split-half correlations, an average five percent is a false positive.

Results

Diversity in Phase Relations

We set out to show reliable diversity in the phase relations between LFP-LFP and LFP-MUA signal pairs recorded in macaque area V4 while the animals were engaged in a perceptual task involving attentional modulation. Importantly, we investigated whether any reliable diversity in the LFP-MUA phase relations could be due to diversity in the MUA-MUA phase relations, because only this diversity can be visible in the receiving downstream areas, namely if the contributing neurons are projection neurons (and not local interneurons).

We examined the phase relations between 96 site pairs from which we obtained both LFP and MUA signals. We calculated the phase relations between 192 ordered LFP-LFP signal pairs and between 192 ordered LFP-MUA signal pairs, with the MUA and the LFP signals always obtained from different sites. Please note that each unordered LFP-LFP channel pair {A,B} appeared twice in the analyses: once in the order (A,B) and once in the reverse order (B,A). This was done in order to investigate the relation between the LFP-LFP channel pairs and the corresponding LFP-MUA channel pairs. All analyses, including the statistical tests, were designed to be free of calculations that produce a symmetry-dependent bias (i.e., a bias that depends on the fact that the LFP-LFP channel pairs appeared in both orders).

We examined the reliability of these phase relations by means of a split-half procedure. In this procedure, we randomly partitioned the trials of each recording session in two groups, and calculated the phase relations separately for each of the two groups of trials. In this way, we obtained two independent estimates of each phase relation. We then plotted these pairs of independent phase relation estimates in scatter plots, separately for the different frequencies. In Figure 2*A,B*, this is shown for eight frequencies: 2.5, 5.5, 11, 19, 26, 55, 87.5, and 120 Hz. In each scatter plot, the pairs of phase relation estimates are color coded by the coherence of this pair, a measure that indexes the consistency of the phase relations over trials.

There was a reliable diversity in the phase relations between the LFPs at different recording sites. Importantly, these recording sites were separated by only 650 or 900 micron (in a plane parallel to the cortical surface). In Figure 1*A* and 1*B*, the diversity of the phase relations is reflected by the length of the cloud of points along the main diagonal of the plot. Importantly, this diversity is only meaningful if the phase relations are also reliable. The reliability of the phase relations is inversely related to the deviations from the main diagonal. If the phase relations were perfectly reliable, then the two independent estimates, from odd and even trials, would be equal and all points would lie exactly on the main diagonal. In contrast, the more *un*reliable the phase relations, the more the two independent estimates would differ, and the more the points would lie scattered in the plot. For most frequencies, the phase relations were very reliable (Fig. 2*A,B*). Note that diversity and reliability are different but related concepts: diversity and reliability can be both high (as for the phase relations at 55 Hz in Fig. 2*B*), diversity can be low and reliability can be high (as for the

phase relations at 19 Hz in Fig. 2*A,B*), and diversity can be high and reliability can be low (all points scattered in the plot; not shown). The two concepts are related in the following way: unreliability implies diversity but not the other way around.

The reliability of the LFP-LFP phase relation estimates by itself is not a particularly interesting phenomenon. In fact, the reliability of these phase relation estimates increases simply as a function of the number of trials, a parameter that is irrelevant for the physiological mechanism that produces these phase relations. The crucial question is whether the reliable phase relation estimates are also diverse. Although absolute reliability is not interesting by itself, it is important to take differences in reliability (over frequencies, conditions, and signal pairs, such as LFP-LFP and LFP-MUA) into account when analyzing these phase relation estimates. This objective was realized in the way in which we quantified phase relation diversity by means of an index (SPHARED, see further).

The diversity of phase relations varied across frequencies and experimental conditions (Fig. 2*A* and 2*B*). There were four experimental conditions in our experiment, which were obtained by crossing the factors *stimulation* (pre-stimulus versus sustained stimulation) and *attention* (inside versus outside the receptive field). See Materials and Methods for details. In the [pre-stimulus, attention inside] condition, phase relation diversity appears to peak once around 11 Hz and once more around 55 and 87.5 Hz (Fig. 2*A*). In the [sustained, attention inside] condition, phase relation diversity appears to peak once around 2.5 Hz and once more around 55 and 87.5 Hz, but not around 11 Hz (Fig. 2*B*). Especially at 55 and 87.5 Hz, phase differences for some pairs of recording sites were very large, ranging from −2 to +2 radians. In the following, we will show that the phase relation diversity at 2.5, 11, 55, and 87.4 Hz represent single points on continuous phase relation diversity spectra, and do not exactly correspond to the peaks of these spectra.

To more easily evaluate how much the phase relations differ across site pairs as a function of frequency and experimental condition, we calculated spectra showing the *across-site-pair (spatial) phase relation diversity* (SPHARED). The SPHARED index is directly linked to the split-half scatter plot: it compares the variability in the phase relation estimates along the line $X = Y$ (with X and Y denoting, resp., the horizontal and the vertical axis) with the variability along the orthogonal line $X = -Y$ (see Fig. 1), and thus measures the amount of *reliable* diversity in the phase relation estimates (see Materials and Methods).

Figure 2*C* shows that the SPHARED spectra had clear peaks, indicating frequency-specific diversity in the phase relations. In the two pre-stimulus conditions (with attention inside or outside the RF), there were peaks of phase relation diversity in the alpha (9–13 Hz) and the gamma (35–75 Hz) band. And in both sustained stimulation conditions (again with attention inside or outside the RF), there were peaks in the low theta (3–4 Hz) and the gamma (35–75 Hz) band.

Although SPHARED is only nonzero if there is reliable diversity in the phase relations, the exact SPHARED also depends on coherence (see Materials and Methods). We also calculated alternative SPHARED indices that do not depend on coherence (see Materials and Methods). These coherence-independent SPHARED spectra showed the same pattern as the original ones (compare Fig. 3*A* and 2*C*). In the following, we will only show these original SPHARED spectra because these are more reliable, especially for analyses that involve LFP-MUA phase relations.

It is informative to compare the SPHARED spectra with their corresponding power spectra (Fig. 3*B*). The peaks and between-condition differences in the power spectra are not a straightforward result of the peaks and between-condition differences in the SPHARED spectra. In the simplest mechanism, power only depends on the degree of lag-zero

synchronization across neuronal space. According to this mechanism, an increase in SPHARED leads to a decrease in power. In contrast, the power spectra show peaks in the low theta (3–4 Hz), alpha (9–13 Hz), beta (18–22 Hz) and the gamma (35–75 Hz) band, and in three of these frequency bands (low theta, alpha and gamma) there are also peaks in the SPHARED spectra. Moreover, except for the low theta band, the between-condition differences in the power spectra are in the opposite direction as expected on the basis of the SPHARED spectra. It follows that, in these recordings, power is not a simple result of the degree of lag-zero synchronization across neuronal space.

The statistical significance of SPHARED was assessed by means of the Pearson correlation coefficient (across all site pairs) between the two sets of phase relation estimates, separately for each of the frequencies. We dealt with the multiple comparison problem (297 frequency-specific p-values) by controlling the false discovery rate (FDR, Benjamini and Hochberg, 1995; Genovese et al., 2002, see Materials and Methods). The frequencies for which the split-half correlations were significant are indicated by the thickness of the line denoting the SPHARED (Fig. 2*C*). For the results shown in Figure 2*C*, all split-half correlations were significant according to the FDR criterion (and therefore all the lines have the same thickness). In other analyses, on which we will report in the following, much more non-significant split-half correlations were found.

Next, we investigated the diversity in the LFP-MUA phase relations. Importantly, we only included LFP-MUA phase relations calculated between different sites. In this way, we avoid the problem that the high-frequency energy in the spikes may leak into the LFPs, and produce artificial coupling between spikes and LFP. Figure 4*A* and 4*B* show split-half scatter plots of the *centered* LFP-MUA phase relations. Centering the LFP-MUA phase relations involved that they were shifted by their mean phase relation, calculated across all LFP-MUA pairs (see Materials and Methods). For almost all frequencies, the average LFP-MUA phase relation was around $4\pi/5$, corresponding to a preferred spiking phase just before the trough of the LFP. Without centering of the phase relations the points in the split-half scatter plots would correspondingly be clustered around ($4\pi/5$, $4\pi/5$). Comparing Figure 4*A* and 4*B* with Figure 2*A* and 2*B*, we see that the LFP-MUA phase relations were less reliable than the LFP-LFP phase relations. However, despite the comparably low reliability of the LFP-MUA phase relations, the SPHARED spectra show clear peaks in the same frequency bands as the LFP-LFP phase relations (Fig. 4*C*), suggesting that LFP-LFP phase relations translate into LFP-MUA phase relations (or vice versa). This diversity in LFP-MUA phase relations differs across the experimental conditions: in the two sustained stimulation conditions, LFP-MUA SPHARED occurred in the low theta (3–4 Hz) and the gamma (35–75 Hz) band, whereas in the two pre-stimulus conditions, they occurred only in the alpha (9–13 Hz) band.

The LFP-MUA SPHARED spectra showed a clear peak in the low theta band (3–4 Hz), but only in the two sustained stimulation conditions. This raises the question whether low theta band SPHARED reflects the rhythm in the drifting square wave luminance gratings (see Visual stimulation and experimental paradigm), which had a frequency between 0.8333 and 1.8750 Hz. However, the largest diversity in the low theta band occurred at 3.5 Hz (Fig. 4*C*), and we therefore believe that this rhythm is intrinsically generated in a condition that involves sustained stimulation. Most likely, this rhythm is coupled to the microsaccades that also occur rhythmically in the same frequency band (Bosman et al., 2009). A further investigation of this hypothesis is beyond the scope of this paper.

It is important to distinguish between two components of the diversity in the LFP-MUA phase relations: (1) diversity across LFP channels for a fixed MUA channel, and (2) diversity across MUA channels for a fixed LFP channel. The latter component can only be

due to diversity in the phase relations between the MUA-MUA channel pairs of which the signals were recorded in the same session in which also the LFP channel was recorded. (Note that all sessions involved four recording sites, and that we only included LFP-MUA phase relations between different recording sites.)

To be visible in the synaptic input to downstream populations, it is crucial that the diversity in the LFP-MUA phase relations at least partly reflects diversity in the MUA-MUA phase relations. We investigated this by quantifying the diversity in the LFP-MUA phase relations *with respect to a fixed* LFP signal. Given that we always recorded LFP and MUA from four sites simultaneously, for each LFP signal we centered at zero the three LFP-MUA phase relations involving this LFP signal (see Materials and Methods). These phase relations will be called *LFP-centered* LFP-MUA phase relations. Diversity in the LFP-centered LFP-MUA phase relations will be reflected in diversity in the MUA-MUA phase relations.

Figure 5A shows split-half scatter plots of LFP-centered LFP-MUA phase relations for the attention inside sustained stimulation condition. At 55 Hz, there was substantial diversity in the LFP-centered LFP-MUA phase relations, but not at other frequencies (Fig. 5A). The same pattern was observed in the other sustained stimulation condition (attention outside) but not in the two pre-stimulus conditions, which did not show phase relation diversity for any of the frequencies (scatter plots not shown).

This pattern of phase relation diversity was also seen in the SPHARED spectra that were calculated from the LFP-centered LFP-MUA phase relations: The phase relation diversity in the two sustained stimulation conditions showed a significant peak in the gamma-frequency band (Fig. 5*B*). The significant LFP-MUA SPHARED after LFP centering demonstrates that the above described LFP-MUA SPHARED is partly reflected in MUA-MUA SPHARED. SPHARED was also significant in other frequency bands and other conditions, but these were very small in number. (Note that, using FDR control at the 0.05-level, it is expected that five percent of the null hypotheses are rejected incorrectly.)

We also investigated MUA-MUA phase relation diversity in a more direct way, starting from phase relations between the MUA-MUA channel pairs, without involving the LFP signals. Using this approach, we did not find significant MUA-MUA phase relation diversity. Most likely, this is due to the unreliability of the MUA-MUA phase relation estimates. This is in line with the much higher coherence in the LFP-MUA as compared to the MUA-MUA channel pairs (Fries et al., 2008).

Diversity in Stimulus-Induced Phase Relation Shifts

The observed frequency-specific phase relation diversity might be due entirely to structural aspects of the neuronal network such as axon length. Alternatively, at least part of the observed phase relation diversity is due to the dynamics of the system. In this case, phase relations should shift to some degree when e.g. visual stimulation changes or when attention shifts from one stimulus to the other. We will first show that the presentation of a stimulus produced reliable and diverse phase relation *shifts*.

This analysis was based on trial-specific estimates of stimulus-induced phase relation shifts. Each trial has a pre-stimulus and a sustained stimulation period, and we calculated the phase relations for each period separately (see Materials and Methods). We then calculated the trial-specific shifts of the sustained-minus-pre-stimulus phase relations, represented these phase relation shifts on the unit-radius complex circle, and then calculated the average of these complex-valued phase relation shifts across trials. This produces a complex number of which the magnitude is a phase-locking factor (PLF, Lachaux et al., 1999) that measures the

across-trial consistency in the stimulus-induced phase relation shifts, and the phase angle gives the preferred phase relation shift.

We evaluated the reliability of the LFP-LFP phase relation shifts using the same tools that were used to evaluate the reliability of the LFP-LFP phase relations: split-half scatter plots (Fig. 6*A*) and spectra of across-site-pair phase-relation-shift diversity (SPHARESD for Spatial PHase RElattion Shift Diversity) (Fig. 6*B*). SPHARESD spectra are calculated in the same way as SPHARED spectra, but using phase relation *shifts* instead of phase relations. There was a reliable diversity in the stimulus-induced LFP-LFP phase relation shifts in exactly the same frequency bands that show reliable LFP-LFP phase relations, namely low theta (roughly 3.6 Hz), alpha (9–13 Hz), and gamma (35–75 Hz). Especially in the gamma band, some phase relation shifts were large, ranging from −1.2 to +1.2 radians (excluding the one outlier pair at −2.4 and +2.4 radians). Relating these observations to the corresponding differences in the SPHARED spectra (Fig. 2*C*), we conclude that the stimulus-induced LFP-LFP phase relation shifts reflect an increase in the phase relation diversity in the low theta and the gamma band, and a decrease in the alpha band.

Next, we examined the diversity in the stimulus-induced LFP-MUA phase relation shifts. We found reliable diversity in the stimulus-induced LFP-MUA phase relation shifts, but only for a small number of LFP-MUA signal pairs, namely those with a high across-trials-consistency in the stimulus-induced LFP-MUA phase relation shifts, as evidenced by a high PLF. These LFP-MUA phase relation shifts were not strong and/or numerous enough to produce an identifiable peak in their SPHARESD spectra. However, when we selected (per frequency) the 10 percent signal pairs with the largest across-trials-consistency in the stimulus-induced LFP-MUA phase relation shifts, we found a very reliable diversity in these stimulus-induced LFP-MUA phase relation shifts (see Fig. 7*A* for the 55 Hz split-half scatter plots with and without selection). This was quantified by the split-half correlations calculated across the selected signal pairs (Fig. 7*B*). For many frequencies, these split-half correlations were significantly different from zero (while controlling the FDR), indicating a reliable diversity in these stimulus-induced LFP-MUA phase relation shifts (Fig. 7*B*). This was most clear for the frequencies between 20 Hz and 80 Hz (Fig. 6*B*). Crucially, these significant split-half correlations are not the result of a biased selection of the signal pairs: the selection of the signal pairs only depended on the *consistency* of the phase relation shifts, and was independent of the size of the phase relation shifts. However, selection on the basis of across-trials-consistency in the LFP-MUA phase relation shifts was necessary to identify significant split-half correlations: when these split-half correlations were calculated across *all* signal pairs, only for one out of 297 frequencies, this correlation was significantly different from zero (figure not shown).

To be visible in the synaptic input to downstream populations, it is crucial that the diversity in the stimulus-induced LFP-MUA phase relation shifts at least partly reflects diversity in the stimulus-induced MUA-MUA phase relation shifts. We investigated this in the same way as for the LFP-MUA phase relations, namely by looking at the diversity in the LFP-centered stimulus-induced LFP-MUA phase relation shifts. As before, for each LFP signal, these LFP-centered phase relation shifts were obtained by centering the three LFP-MUA phase relation shifts such that their average was zero. Diversity in the LFP-centered stimulus-induced LFP-MUA phase relations shifts reflects diversity in the stimulus-induced MUA-MUA phase relation shifts.

We found a similar pattern as in the non-LFP-centered stimulus-induced LFP-MUA phase relation shifts: reliable stimulus-induced LFP-centered LFP-MUA phase relation shifts, but only for a small number of LFP-MUA signal pairs, not producing an identifiable peak in their SPHARESD spectra. However, these shifts were clearly visible in the split-half

correlations calculated across the 10 percent signal pairs with the largest consistency in the stimulus-induced LFP-MUA phase relation shifts (see Fig. 8*A* for the 55 Hz split-half scatter plots with and without selection). Predominantly for the gamma (35–75 Hz) band, these split-half correlations were significantly different from zero, indicating a reliable diversity in the LFP-centered stimulus-induced LFP-MUA phase relation shifts (Fig. 8*B*) and therefore also a reliable diversity in the stimulus-induced MUA-MUA phase relation shifts. Thus, the diversity in the MUA-MUA phase relation shifts is responsible for part of the diversity in the LFP-MUA phase relation shifts.

We also investigated diversity in the stimulus-induced MUA-MUA phase relation shifts in a more direct way, using the stimulus-induced MUA-MUA phase relation shifts, without involving the LFP signals. Using this approach, we did not find significant diversity in the stimulus-induced MUA-MUA phase relation shifts, which is most likely due to the unreliability of their estimates.

In summary, the analysis of stimulus induced phase-relation shifts demonstrated that the phase relation diversity observed under a given stimulus condition does not simply reflect structural aspects of the neuronal network but can change in response to stimuli.

Diversity in Attention-Induced Phase Relation Shifts

We will now show that the phase relations also reflect the direction of attention (i.e., attention inside versus outside the receptive field). We started our calculations by grouping the trials in pairs such that each pair contained one trial in which attention was directed inside the receptive field, and one trial in which it was directed outside the receptive field. In this, the pairing of a particular attention-in trial with a particular attention-out trial was arbitrary and only for analysis purposes. For each pair of trials, we calculated the attention-induced phase relation shift (see Materials and Methods), separately for the pre-stimulus and the sustained stimulation period. In the same way as for the stimulus-induced phase relation shifts, we then calculated the trial-pair-specific inside-minus-outside phase relation shifts, represented these phase relation shifts on the unit-radius complex circle, and then calculated the trial-average of these complex-valued phase relation shifts. This produces a complex number of which the magnitude is a PLF that measures the across-trial consistency in the attention-induced phase relation shifts. The phase angle of this complex trial-average measures the preferred phase relation shift.

We evaluated the reliability of the attention-induced LFP-LFP phase relation shifts using split-half scatter plots (Fig. 9*A*) and SPHARESD spectra (Fig. 9B). In Figure 9*A*, we only show the scatter plot for the pre-stimulus condition; the one for the sustained stimulation condition is highly similar. Note the different scales of the split-half scatter plots in Fig. 9 as compared to Fig. 6. The attention-induced LFP-LFP phase relation shifts (from −0.35 to +0.35 radians) are notably smaller than the stimulus-induced LFP-LFP phase relation shifts (from −1.2 to +1.2 radians). There was a reliable diversity in the attention-induced LFP-LFP phase relation shifts in the gamma (35–75 Hz) band. Some frequencies outside of the gamma band also exhibited reliable diversity, but these frequencies did not form such a broad contiguous frequency band as the diversity in the gamma band.

Next, we examined the diversity in the attention-induced LFP-MUA phase relation shifts. We found reliable diversity in attention-induced LFP-MUA phase relation shifts, but only for the LFP-MUA signal pairs with a high across-trials-consistency in the attention-induced LFP-MUA phase relation shifts. Moreover, different from the *stimulus*-induced LFP-MUA phase relation shifts, there was not a convincing spectral pattern in the split-half correlations that were used to evaluate this diversity; frequencies with a reliable diversity were scattered across multiple narrow frequency bands (figures not shown).

Discussion

We investigated (1) whether there is reliable across-site-pair diversity in the LFP-LFP and the LFP-MUA phase relations, and (2) whether this diversity is affected by the presence of a stimulus, as well as by a cognitive variable, selective attention. We found that in three discrete frequency bands (low theta, alpha, and gamma), there was substantial and reliable diversity in the phase relations between LFP signals. We also found that the corresponding LFP-MUA phase relations showed diversity in the same three frequency bands. Crucially, for the gamma band, this diversity in the LFP-MUA phase relations was partly due to diversity in the MUA-MUA phase relations. This is a necessary condition for the phase relations to be also visible in downstream areas. Further, we found that the presentation of a visual stimulus in the receptive field of the recorded neuronal population produced reliable shifts in the LFP-LFP phase relations in the same three frequency bands (low theta, alpha, and gamma). We also found reliable diversity in the stimulus-induced LFP-MUA phase relation shifts, but only for the channel pairs with highly consistent phase relation shifts and predominantly in the gamma band. Importantly, for the gamma band, this diversity in the stimulus-induced LFP-MUA phase relation shifts was partly due to diversity in the MUA-MUA phase relation shifts. Finally, we also found that not only visual stimulation but also covert selective attention to a visual stimulus produced reliable shifts in the LFP-LFP phase relations. Contrary to the effect of visual stimulation on the LFP-LFP phase relations, the effect of selective attention was confined to the gamma band.

Several previous studies investigated diversity in phase relations between neuronal activity recorded at multiple sites. Travelling waves, for instance, are a well-known special case of SPHARED. Travelling waves are essentially SPHARED with a particular phase relationship between neighboring sites. Travelling waves have been observed in several model systems, such as the central olfactory organs in a number of species (Freeman, 1978; Delaney et al., 1994; Lam et al., 2000), turtle visual cortex (Prechtl et al., 1997; Prechtl et al., 2000), rat hippocampus (Lubenov and Siapas, 2009), and macaque motor cortex (Rubino et al., 2006). In a recent study, van der Meij et al (2012) demonstrated SPHARED in phase-amplitude coupling. This study showed that most of the spatial diversity in the preferred coupling phases is due to phase relation diversity in the spatially distributed slow oscillation to which the amplitudes of the fast oscillations are coupled.

Our results complement a recent study by Havenith et al (2011) in anesthetized cat visual cortex, that showed the existence of single unit preferred firing sequences (i.e., reliable timing differences) and, importantly, the change of these sequences as a function of stimulus properties. Crucially, these firing sequences are referenced not to external events but to ongoing LFP oscillations in the beta and the gamma band. We also observed reliable timing differences between spiking activity, but now in MUA signals recorded at different sites. Similar to the study by Havenith et al (2011), these timing differences are visible in diverse LFP-MUA phase relations in the gamma band. However, different from Havenith et al (2011), we also observed diversity in the LFP-LFP phase relations (see Fig. 2, 5, and 7), and found this diversity in three discrete frequency bands. Importantly, exactly the same frequency bands also showed diversity in the LFP-MUA phase relation (see Fig. 4).

Our results also complement a recent study by Vinck et al. (2010; see also, Womelsdorf et al., 2012), who showed stimulus-induced LFP-single-unit phase relation shifts in V1. In fact, these authors showed that visual stimuli that increase a neuron's firing rate also advance its preferred spiking phase in the LFP-defined gamma cycle. In our study, we showed that LFP-MUA phase relation diversity not only reflects diversity in stimulus properties, but is also present *within* the different stimulus conditions (i.e., pre-stimulus and sustained stimulation; see Fig. 4). Interestingly, the study byVinck et al. (2010) showed that only part of the

diversity in LFP-single- unit phase relations could be explained by between-unit differences in firing rate that resulted from a manipulation of stimulus orientation (see Fig. 3 in Vinck et al., 2010). Another recent study investigating the effect of luminance contrast on LFP-single-unit phase relations in awake monkey V1 failed to find contrast-related shifts in LFP-single unit phase relations (Ray and Maunsell, 2010).

Siegel et al. (2009) investigated the modulation of LFP-MUA phase relations by a cognitive variable: short-term memory content. These authors demonstrated phase-dependent object coding in prefrontal cortex: optimal spike rate encoding for the first memorized object occurred in an earlier phase of a beta band oscillation than for the second memorized object. This study and the one byVinck et al. (2010) demonstrate that the phase relations between LFPs and spikes (both MUA and single units) can carry information about a cognitive variable and about stimulus properties. This confirms our observation of stimulus-induced SPHARESD.

We showed SPHARED and SPHARESD in three non-overlapping frequency bands: low theta (3–4 Hz), alpha (9–13 Hz), and gamma (35–75 Hz). Whereas many studies in visual cortex showed neuronal oscillations in the alpha and the gamma band, very few have shown oscillations in the low theta band. In this context, it is surprising to see the very large 3.5 Hz SPHARED in the LFP-MUA channel pairs. Possibly, this rhythm is the same as the one that has been shown to be coupled to micro-saccades that also occur rhythmically in the same frequency band (Bosman et al., 2009). This supports the hypothesis that this low theta rhythm plays a role in the way we sample visual input from our environment.

From the fact that LFP-LFP and LFP-MUA phase relations are modulated by stimulation as well as by selective attention, we conclude that they inform us about neuronal information processing. Although this is an interesting observation as such, it is not sufficient evidence for a mechanism via which phase relations affect neuronal spiking, which is the signal for targeted communication between neurons. Additional evidence for phase relations affecting neuronal spiking is the diversity in the LFP-centered LFP-MUA phase relations, which reflects diversity in the MUA-MUA phase relations. Assuming that also projection neurons contribute to the MUA, this diversity is also visible in the synaptic input to downstream populations. In the same way, the LFP-centered stimulus-induced LFP-MUA phase relation *shifts* reflects the fact that this stimulus also shifts the MUA-MUA phase relations. Again assuming the contribution of projection neurons to the MUA, these stimulus-induced shifts must also be visible in the synaptic input to downstream populations. Importantly, we found this evidence only for a subset of LFP-MUA channel pairs, those with very consistent LFP-MUA phase relation shifts, and only in the gamma band.

It is important to be aware that these phase relations were observed across recording sites that were separated by only 650 or 900 micron. Moreover, the receptive fields (RFs) of these recording sites overlapped substantially. Despite the short inter-electrode distances and the RF overlap, there was a substantial diversity in the phase relations and their between-condition shifts. What causes the diversity in the phase relations and their shifts? To answer this question, we distinguish between the phase relations and their shifts. Phase relation diversity *within* a condition can be explained by structural aspects, such as the layers from which the signals are recorded or the neuron types (e.g., excitatory or inhibitory) that contribute to these signals. Livingstone (1996) investigated visually induced gamma-band synchronization between single unit spikes recorded in squirrel monkey V1 within one cortical column, at different cortical depths. She reports that across the layers 4B, 3 and 2, the deeper single unit precedes the more superficial single unit. The temporal delay appears to be directly related to vertical cortical distance, with any 400 micron distance, irrespective of layer boundaries, resulting in a delay of roughly 3 ms. She points out that this temporal

relationship is consistent with the flow of information. These results are fully consistent with the findings presented here, and they suggest that at least part of the phase relation diversity is due to different cortical recording depths and the corresponding synaptic distances from layer 4, the cortical input layer.

Diversity in phase relation *shifts* between conditions (prestimulus versus sustained stimulation, and attention inside versus outside the receptive field) cannot be explained by these structural aspects, but rather require neuronal activation-related mechanisms. While the precise phase relation shift mechanisms are currently still unknown, several suggestions can be made based on previous studies. To better understand these mechanisms, it is important to ask whether the phase relation shifts could be a simple byproduct of other differences between conditions. We will consider this question first for the LFP-LFP and then for the LFP- MUA phase relation shifts. For the LFP-LFP phase relation shifts, it must be asked whether and how much of the phase relation shifts are the result of changes in oscillatory amplitude. In fact, the observed oscillatory neural activity may be produced by multiple oscillatory sources with non-zero phase relations. Different recording electrodes deliver signals that are different linear mixtures of these multiple sources, with the weights of these mixtures being proportional to their distance from the sources (Nunez and Srinivasan, 2006). Crucially, the phase relations between the recording electrodes depend on (1) the weights of these linear mixtures and (2) the relative amplitudes of the oscillatory sources. In this scenario, changes in these relative amplitudes (e.g., induced by a stimulus) will also produce changes in the phase relations. Thus, it cannot be excluded that oscillatory amplitude is the relevant physiological variable (in the sense that it causes changes in neural activity in downstream areas) and the LFP-LFP phase relation shifts could thus be an inconsequential byproduct.

Our conclusion is different when we consider the LFP-MUA phase relation shifts. Crucially, we found diversity in the LFP-centered LFP-MUA phase relation shifts, which reflects diversity in the MUA-MUA phase relation shifts. Thus, a stimulus induces MUA-MUA phase relation shifts. There are multiple plausible mechanisms for such MUA-MUA phase relation shifts, and in the following, we briefly describe two. These mechanisms depend on several cellular and network-level phenomena that are an active area of investigation, but of which only a subset has been demonstrated. In one putative mechanism, MUA-MUA phase relation shifts emerge from an interaction of rhythmic inhibition with varying levels of excitation. An activated local basket cell network generates gamma and imposes the corresponding rhythmic inhibition onto the other neurons in the local network. The excitatory neurons spike when their excitation exceeds the inhibition (Fries et al., 2007; Vinck et al., 2010). Correspondingly, changes in relative excitation levels lead to changes in spike timing and corresponding phase relation shifts.

In a second mechanism, MUA-MUA phase relation shifts emerge from an interaction of different gamma-frequencies with a rhythmic phase reset. Several studies have demonstrated the existence of different gamma-band peak frequencies within a single animal. Specifically, the gamma-band peak frequency increases with stimulus contrast (Ray and Maunsell, 2010) and selective attention (Bosman et al., 2012), and decreases with stimulus size (Gieselmann and Thiele, 2008; Ray and Maunsell, 2011) and stimulus composition (Lima et al., 2010). Heterogeneity in gamma-band peak frequency has also been shown in closely neighboring areas (Ray and Maunsell, 2010). Combined with a rhythmic reset of gamma phase (e.g., in the theta-band, as in Bosman et al., 2012), this heterogeneity will produce heterogeneity in the phase relations: after a gamma-phase reset, a faster local gamma rhythm will precess against a slower local gamma rhythm, leading to a certain mean phase relation across the cycle of the rhythmic phase resetter. Changing stimulation and/or attention conditions could change the precise local gamma frequencies and should thereby lead to phase-relation shifts.

Assuming the contribution of projection neurons to the MUA, the MUA-MUA phase relation shifts also affect downstream populations. This fact does not rule out that the MUA-MUA phase relation shifts may be the result of a process that also involves modulations of other physiological variables, such as relative oscillatory amplitudes. The possible dependence of the phase relations on the relative oscillatory amplitudes, by itself, does not make them an irrelevant by-product; it may even hold that changes in the relative amplitudes (in part) affect downstream neurons via the induced MUA-MUA phase relation shifts. In sum, regardless of the mechanism that produces MUA-MUA phase relation shifts, assuming the contribution of projection neurons, these shifts will have downstream consequences.

The next question is how phase relation shifts are relevant for neuronal communication. A core motif in neuronal communication is that of a downstream neuronal population (e.g., area IT) that is flexibly driven by one of multiple upstream populations (e.g., multiple V4 subareas) depending on task demands (Fries, 2005; Womelsdorf et al., 2007; Bosman et al., 2012). The selection of this driving upstream population could depend on the pattern of phase relations between these upstream populations. Multiple mechanisms are conceivable that can all perform selection of the driving upstream population. The mechanisms that have been proposed until now do not explicitly consider diversity in the phase relations between upstream populations. For instance, the communication through coherence (CTC) hypothesis (Fries, 2005) states that selection is determined by the pattern of synchronization between upstream and downstream populations (see also, Tiesinga and Sejnowski, 2009). According to CTC, a pair of communicating up- and downstream populations is coherent with a phase relation that is such that the synaptic input arrives at an excitable phase of the downstream population. On the other hand, a pair of *non*-communicating up- and downstream populations is either non-coherent or has a phase relation that is such that the synaptic input arrives at a *non*-excitable phase of the downstream population. This second variant of CTC shows the possible functional role of phase relation diversity across multiple upstream populations. However, it does not propose phase relation diversity as a mechanism that selects communicating up- and downstream populations.

Our study calls for the formulation of selection mechanisms that make use of the spike timing relations that are implied by the observed phase relation diversity. Obvious ingredients of such timing-based selection mechanisms are cellular and local network properties such as the refractory period and inhibition by local interneurons (Tiesinga et al., 2008). A recent study has demonstrated that the dendritic tree integrates synaptic input in a nonlinear way, such that different input sequences are distinguished (Branco et al., 2010). This could function as a mechanism by which even the single neuron can perform timing-based selection. The investigation of such putative mechanisms requires the simultaneous recording from communicating up- and downstream populations.

Independent of the functional significance of the observed phase relation diversity, it is an interesting data aspect from the perspective of decoding brain activity. In fact, the coding space drastically increases by considering properties of channel *pairs* (i.e., their phase relations) instead of properties of single channels (e.g., their amplitudes or their phases relative to some fixed event). For example, with 50 channels, there are 1225 channel pairs. The attention-induced phase relation shifts that were observed in this study (Fig. 9) are a first step towards this type of application.

References

Benjamini Y, Hochberg Y. Controlling the false discovery rate - A practical and powerful approach to multiple testing. J Roy Stat Soc B Met. 1995; 57:289–300.

Bosman C, Schoffelen J-M, Brunet N, Oostenveld R, Bastos A, Womelsdorf T, Rubehn B, Stieglitz T, De Weerd P, Fries P. Attentional stimulus selection through selective synchronization between monkey visual areas. Neuron. 2012; 75:875–888. [PubMed: 22958827]

Bosman CA, Womelsdorf T, Desimone R, Fries P. A Microsaccadic Rhythm Modulates Gamma-Band Synchronization and Behavior. Journal of Neuroscience. 2009; 29:9471–9480. [PubMed: 19641110]

Branco T, Clark B, Häusser M. Dendritic discrimination of temporal input sequences in cortical neurons. Science (New York, NY). 2010; 329:1671–1675.

Buzsaki G, Draguhn A. Neuronal oscillations in cortical networks. Science. 2004; 304:1926–1929. [PubMed: 15218136]

Delaney KR, Gelperin A, Fee MS, Flores JA, Gervais R, Tank DW, Kleinfeld D. Waves and stimulus-modulated dynamics in an oscillating olfactory network. Proceedings of the National Academy of Sciences of the United States of America. 1994; 91:669–673. [PubMed: 8290580]

Engel AK, Fries P, Singer W. Dynamic predictions: Oscillations and synchrony in topdown processing. Nature Reviews Neuroscience. 2001; 2:704–716.

Freeman WJ. Spatial properties of and EEG event in olfactory-bulb and cortex. Electroencephalography and Clinical Neurophysiology. 1978; 44:586–605. [PubMed: 77765]

Fries P. A mechanism for cognitive dynamics: neuronal communication through neuronal coherence. Trends in Cognitive Sciences. 2005; 9:474–480. [PubMed: 16150631]

Fries P, Nikolic D, Singer W. The gamma cycle. Trends in Neurosciences. 2007; 30:309–316. [PubMed: 17555828]

Fries P, Reynolds JH, Rorie AE, Desimone R. Modulation of oscillatory neuronal synchronization by selective visual attention. Science. 2001; 291:1560–1563. [PubMed: 11222864]

Fries P, Womelsdorf T, Oostenveld R, Desimone R. The effects of visual stimulation and selective visual attention on rhythmic neuronal synchronization in macaque area v4. Journal of Neuroscience. 2008; 28:4823–4835. [PubMed: 18448659]

Genovese CR, Lazar NA, Nichols T. Thresholding of Statistical Maps in Functional Neuroimaging Using the False Discovery Rate. NeuroImage. 2002; 15:870–878. [PubMed: 11906227]

Gieselmann M, Thiele A. Comparison of spatial integration and surround suppression characteristics in spiking activity and the local field potential in macaque V1. The European journal of neuroscience. 2008; 28:447–459. [PubMed: 18702717]

Havenith MN, Yu S, Biederlack J, Chen NH, Singer W, Nikolic D. Synchrony Makes Neurons Fire in Sequence, and Stimulus Properties Determine Who Is Ahead. Journal of Neuroscience. 2011; 31:8570–8584. [PubMed: 21653861]

Jarvis MR, Mitra PP. Sampling properties of the spectrum and coherency of sequences of action potentials. Neural Computation. 2001; 13:717–749. [PubMed: 11255566]

Lachaux JP, Rodriguez E, Martinerie J, Varela FJ. Measuring phase synchrony in brain signals. Human Brain Mapping. 1999; 8:194–208. [PubMed: 10619414]

Lam YW, Cohen LB, Wachowiak M, Zochowski MR. Odors elicit three different oscillations in the turtle olfactory bulb. Journal of Neuroscience. 2000; 20:749–762. [PubMed: 10632604]

Lima B, Singer W, Chen N-H, Neuenschwander S. Synchronization dynamics in response to plaid stimuli in monkey V1. Cerebral cortex (New York, NY). 2010; 1991; 20:1556–1573.

Livingstone M. Oscillatory firing and interneuronal correlations in squirrel monkey striate cortex. Journal of Neurophysiology. 1996; 75:2467–2552. [PubMed: 8793757]

Lubenov EV, Siapas AG. Hippocampal theta oscillations are travelling waves. Nature. 2009; 459:534–539. [PubMed: 19489117]

Mitra PP, Pesaran B. Analysis of dynamic brain imaging data. Biophys J. 1999; 76:691–708. [PubMed: 9929474]

Murthy VN, Fetz EE. Coherent 25-HZ to 35-HZ oscillations in the sensorimotor cortex of awake behaving monkeys. Proceedings of the National Academy of Sciences of the United States of America. 1992; 89:5670–5674. [PubMed: 1608977]

Nunez PL, Srinivasan R. Electric fields of the brain: the neurophysics of EEG. Oxford University Press, USA. 2006

Pesaran B, Pezaris JS, Sahani M, Mitra PP, Andersen RA. Temporal structure in neuronal activity during working memory in macaque parietal cortex. Nature Neuroscience. 2002; 5:805–811.

Prechtl JC, Bullock TH, Kleinfeld D. Direct evidence for local oscillatory current sources and intracortical phase gradients in turtle visual cortex. Proceedings of the National Academy of Sciences of the United States of America. 2000; 97:877–882. [PubMed: 10639173]

Prechtl JC, Cohen LB, Pesaran B, Mitra PP, Kleinfeld D. Visual stimuli induce waves of electrical activity in turtle cortex. Proceedings of the National Academy of Sciences of the United States of America. 1997; 94:7621–7626. [PubMed: 9207142]

Ray S, Maunsell JHR. Differences in Gamma Frequencies across Visual Cortex Restrict Their Possible Use in Computation. Neuron. 2010; 67:885–896. [PubMed: 20826318]

Ray S, Maunsell J. Different origins of gamma rhythm and high-gamma activity in macaque visual cortex. Plos Biology. 2011; 9

Rubino D, Robbins KA, Hatsopoulos NG. Propagating waves mediate information transfer in the motor cortex. Nature Neuroscience. 2006; 9:1549–1557.

Schroeder CE, Lakatos P. Low-frequency neuronal oscillations as instruments of sensory selection. Trends in Neurosciences. 2009; 32:9–18. [PubMed: 19012975]

Tiesinga P, Sejnowski TJ. Cortical Enlightenment: Are Attentional Gamma Oscillations Driven by ING or PING? Neuron. 2009; 63:727–732. [PubMed: 19778503]

Tiesinga P, Fellous JM, Sejnowski TJ. Regulation of spike timing in visual cortical circuits. Nature Reviews Neuroscience. 2008; 9:97–109.

van der Meij R, Kahana M, Maris E. Phase-amplitude coupling in human ECoG is spatially distributed and phase diverse. Journal of Neuroscience. 2012; 32:111–123. [PubMed: 22219274]

Vinck M, Lima B, Womelsdorf T, Oostenveld R, Singer W, Neuenschwander S, Fries P. Gamma-Phase Shifting in Awake Monkey Visual Cortex. Journal of Neuroscience. 2010; 30:1250–1257. [PubMed: 20107053]

Wang X, Ding MZ. Relation between P300 and event-related theta-band synchronization: A single-trial analysis. Clinical Neurophysiology. 2011; 122:916–924. [PubMed: 20943435]

Womelsdorf T, Fries P. The role of neuronal synchronization in selective attention. Current Opinion in Neurobiology. 2007; 17:154–160. [PubMed: 17306527]

Womelsdorf T, Schoffelen JM, Oostenveld R, Singer W, Desimone R, Engel AK, Fries P. Modulation of neuronal interactions through neuronal synchronization. Science. 2007; 316:1609–1612. [PubMed: 17569862]

Womelsdorf T, Lima B, Vinck M, Oostenveld R, Singer W, Neuenschwander S, Fries P. Orientation selectivity and noise correlation in awake monkey area V1 are modulated by the γ cycle. Proceedings of the National Academy of Sciences of the United States of America. 2012; 109:4302–4307. [PubMed: 22371570]

Highlights

- Across site pairs, LFP-LFP and LFP-MUA phase relations differ and are very reliable.
- Visual stimulation and attention induce reliable shifts in these phase relations.
- This may reflect mechanisms that use time relations for the routing of information.

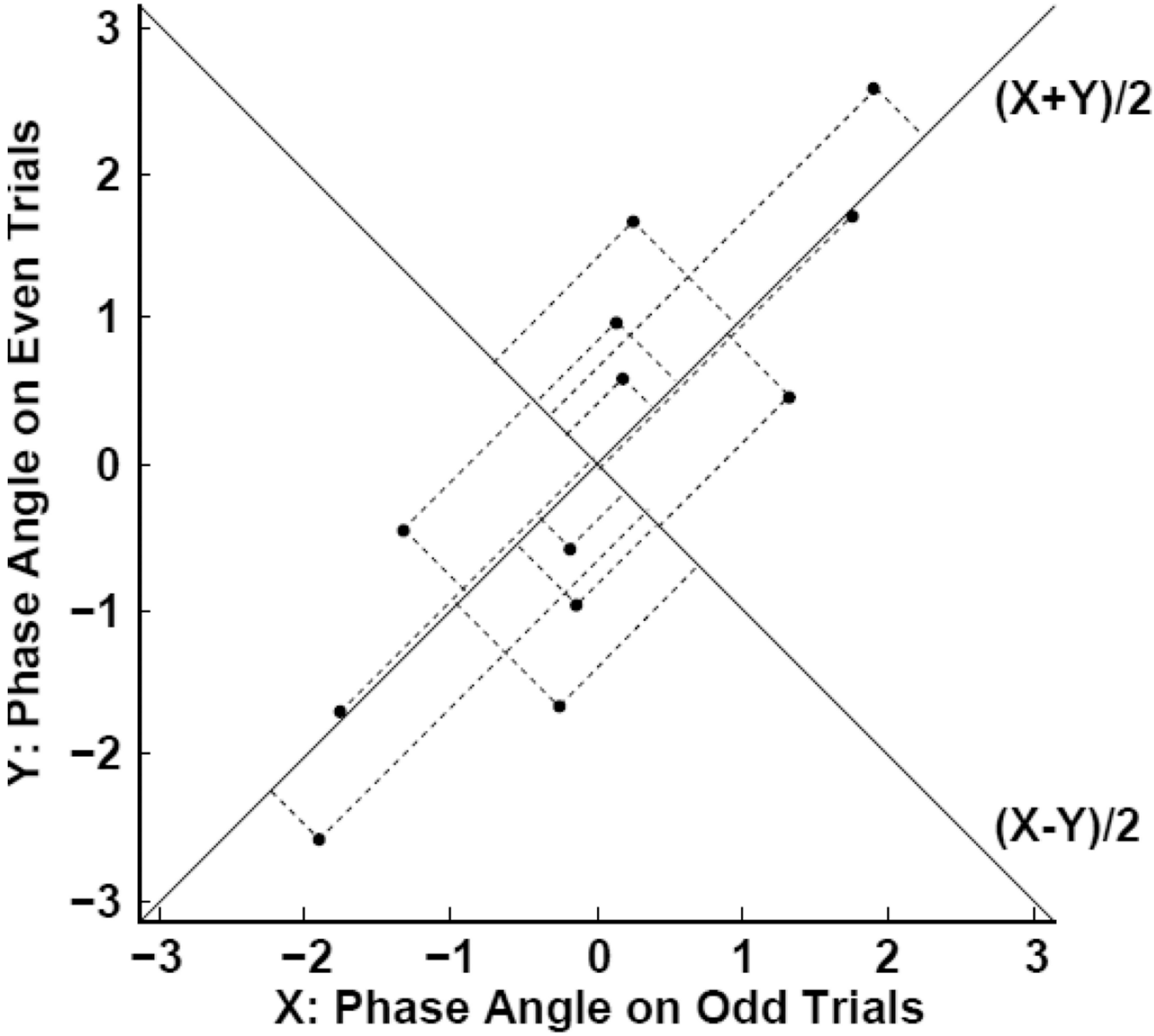

Figure 1. Calculation of the across-site-pair phase relation diversity (SPHARED)

The horizontal axis of the scatter plot (*X*) shows the phase relations calculated on the odd-numbered trials, and the vertical axis (*Y*) shows the phase relations calculated on the even-numbered trials. Each point in the scatter plot is projected on an alternative set of coordinate axes represented by the lines $(X + Y)/2$ and $(X - Y)/2$. The diversity in the phase relations (both reliable and unreliable) is indexed by the variability in the projections on the coordinate axis $(X + Y)/2$. The unreliable diversity in the phase relations is indexed by the variability in the projections on the coordinate axis $(X - Y)/2$. The variability along both $(X + Y)/2$ and $(X - Y)/2$ are both quantified by weighted phase-locking factors and the SPD is obtained as the difference between these two (see Eq. 1).

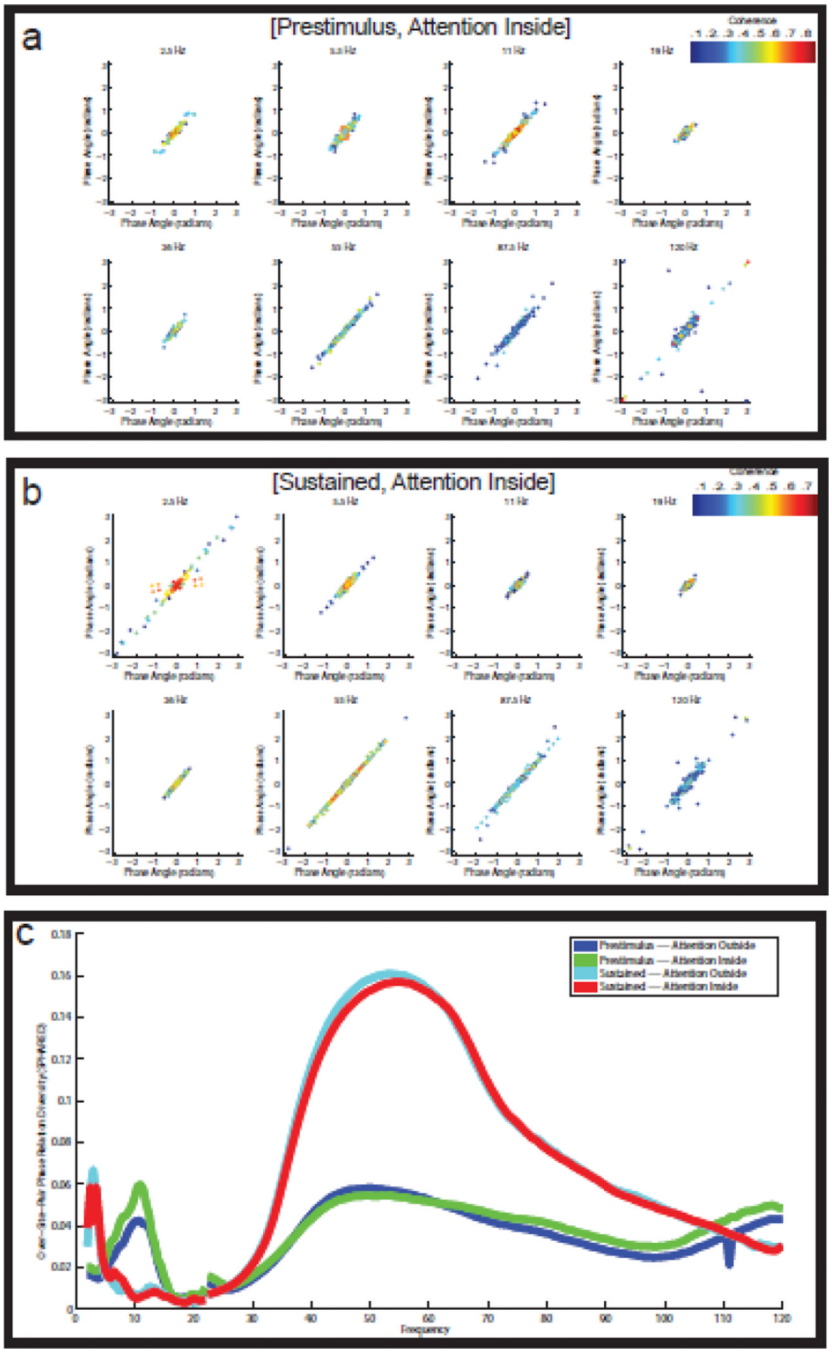

Figure 2. Reliable diversity in the LFP-LFP phase relations

(a) Split-half scatter plots of the LFP-LFP phase relations for eight different frequencies in the [pre-stimulus, attention inside] condition. The horizontal axis shows the phase relations calculated on the even-numbered trials, and the vertical axis shows the phase relations calculated on the odd-numbered trials. The points in the scatter plots are color-coded according to the coherence of the corresponding channel pair. Large reliable phase relations occur at 11 Hz and at 55 Hz. (b) Split-half scatter plots of the LFP-LFP phase relations for eight different frequencies in the [sustained, attention inside] condition. Large reliable phase relations occur at 2.5 Hz and at 55 Hz, but not at 11 Hz. Especially at 55 Hz, the phase relations can be very large, ranging from −2 to +2 radians. (c) SPHARED spectra (see

Materials and Methods) for the four experimental conditions. The SPHARED coefficients measure the reliable diversity in the phase relations. In the two pre-stimulus conditions, there is phase relation diversity in the alpha (9–13 Hz) and the gamma (35–75 Hz) band. And in both sustained stimulation conditions, there is phase relation diversity in the low theta (3–4 Hz) and the gamma (35–75 Hz) band. Statistical significance (with FDR-correction) is indicated by the thickness of the lines.

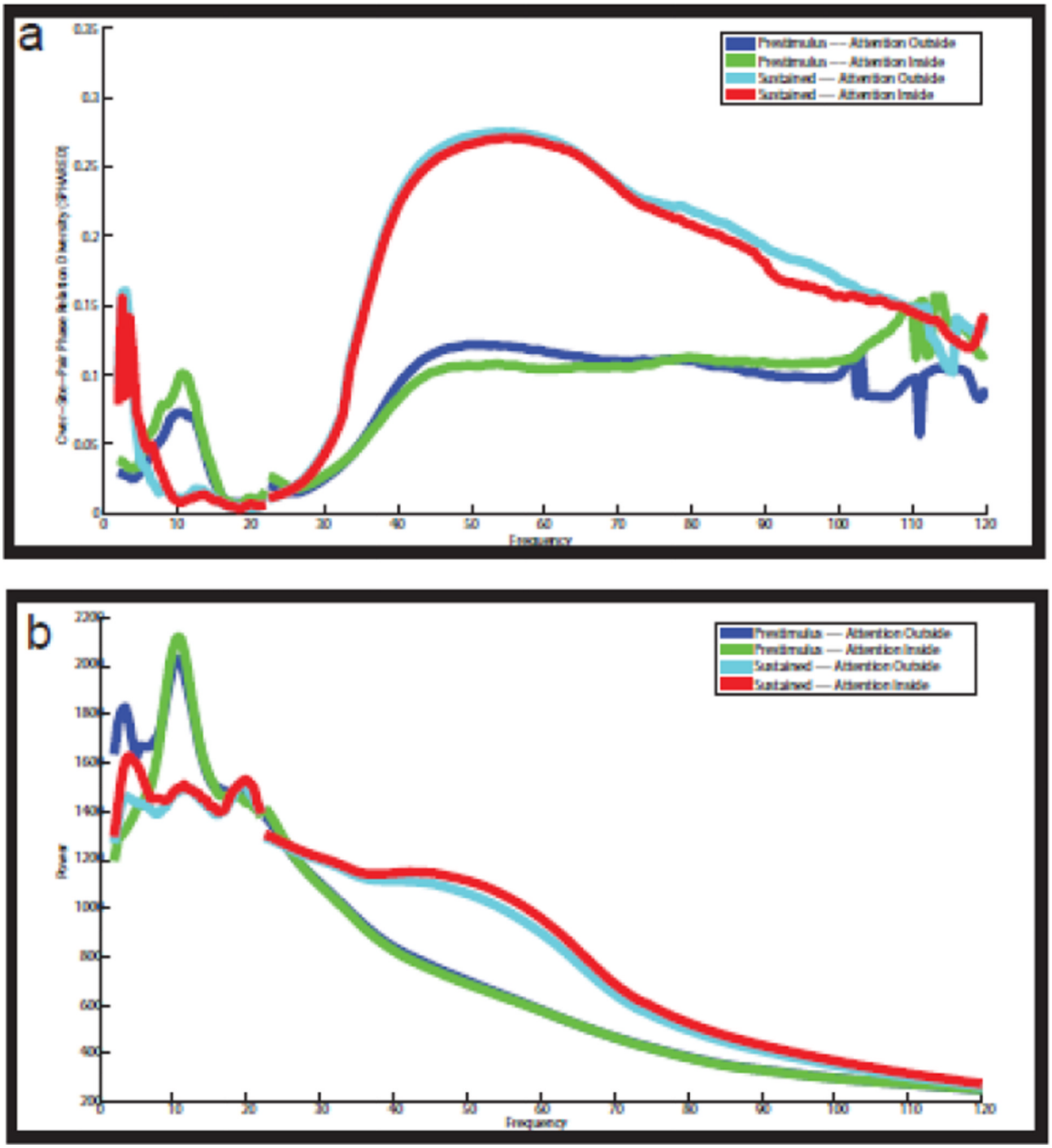

Figure 3. Coherence-normalized SPHARED spectra and a comparison between the SPHARED and the power spectra

(a) Coherence-normalized SPHARED spectra of the LFP-LFP phase relations for the four experimental conditions. These spectra show the same pattern as the original (non-normalized) SPHARED spectra (compare Fig. 3*A* and 2*C*). (b) Power spectra of the LFP channels for the four experimental conditions. These power spectra show peaks in the low theta (3–4 Hz), alpha (9–13 Hz), beta (18–22 Hz) and the gamma (35–75 Hz) band. In three of these frequency bands (low theta, alpha and gamma), there are also peaks in the SPHARED spectra. Therefore, power is not a simple result of the degree of lag-zero

synchronization across neuronal space (see text). The same is concluded from the between-condition differences in the power spectra (see text).

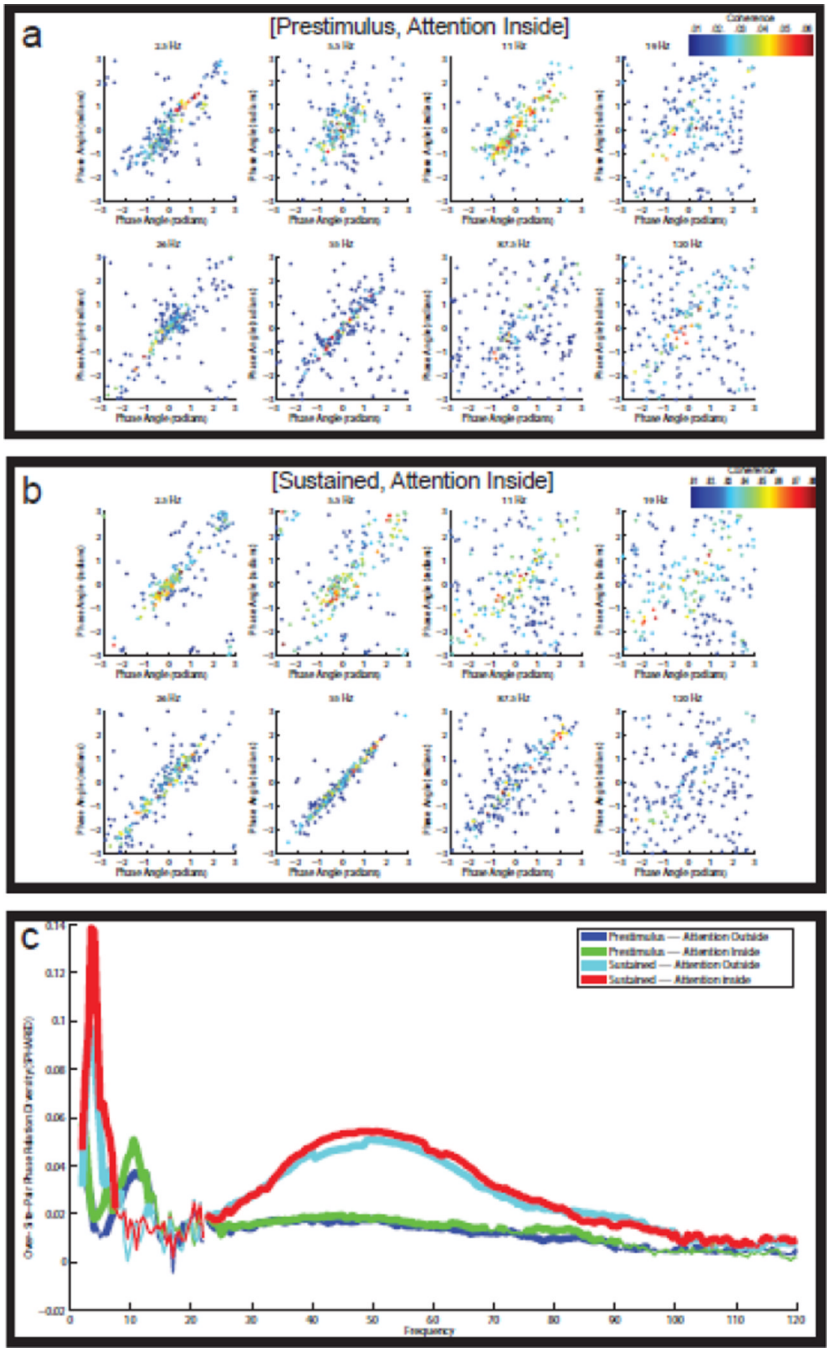

Figure 4. Reliable diversity in the LFP-MUA phase relations

See the caption of Figure 2, which shows the results for the LFP-LFP channels. The main difference with Figure 2 is that the LFP-MUA phase relations are centered, which involves that they were shifted by their average phase relation, as calculated over all LFP-MUA pairs (see Materials and Methods). As compared to the LFP-LFP phase relations, the LFP-MUA phase relations are less reliable. However, despite this relative unreliability, the SPHARED spectra show clear peaks at exactly the same frequency bands as the SPHARED spectra for the LFP-LFP phase relations.

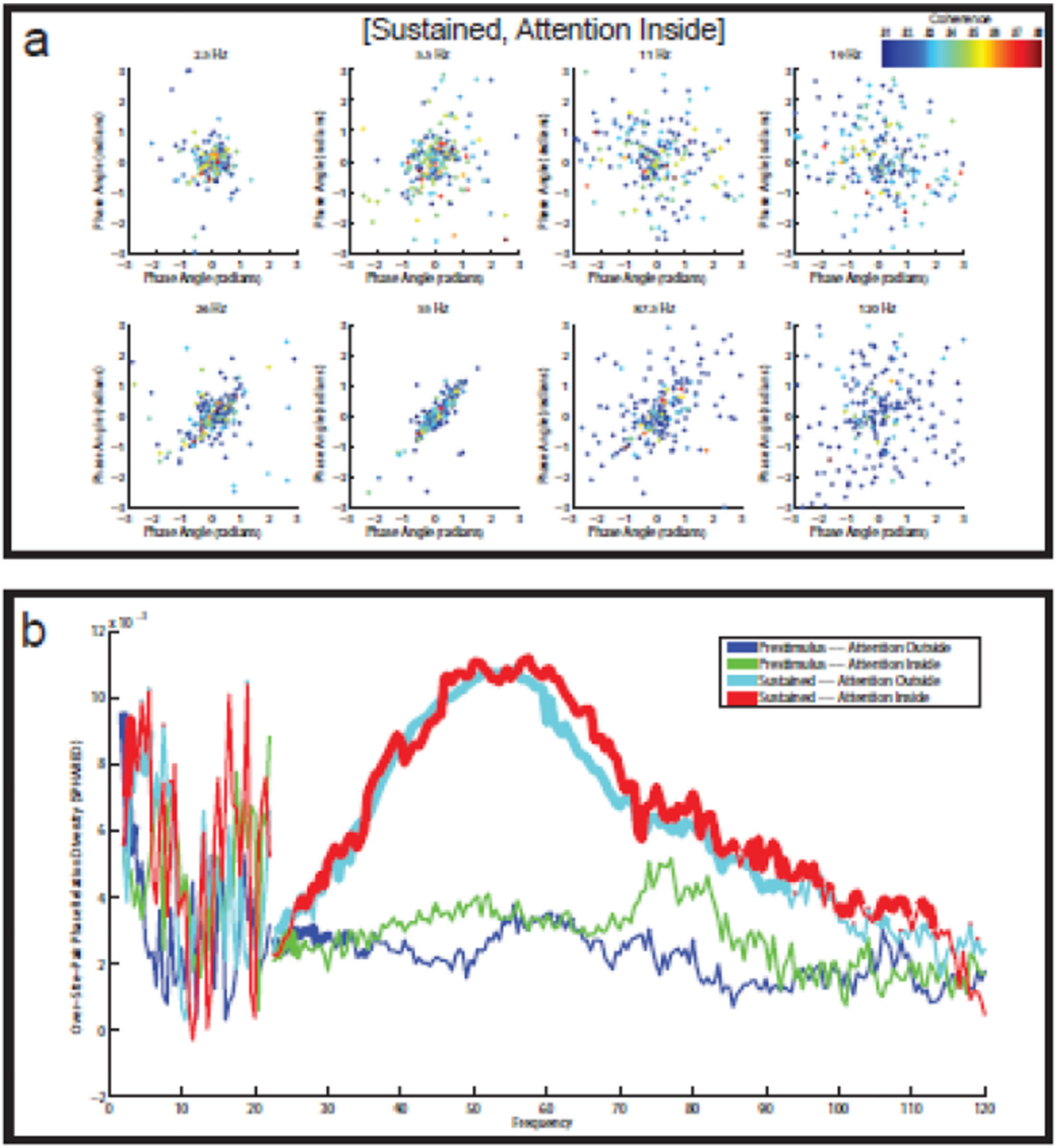

Figure 5. Reliable diversity in the LFP-centered LFP-MUA phase relations

See the caption of Figure 3. The main difference with Figure 3 is that the LFP-MUA phase relations are now centered in an LFP-channel-specific way: phase relations were shifted by the average phase relation calculated over the three LFP-MUA channel pairs that involve the same LFP channel (see Materials and Methods). (a) Split-half scatter plots of the LFP-centered LFP-MUA phase relations for eight different frequencies in the [pre-stimulus, attention inside] condition. At 55 Hz, there was substantial diversity in the LFP-centered LFP-MUA phase relations. (b) SPHARED spectra for the four experimental conditions, calculated on the LFP-centered LFP-MUA phase relations. There was significant gamma

band (35–75 Hz) phase relation diversity in the two sustained stimulation conditions, but not in the two pre-stimulus conditions.

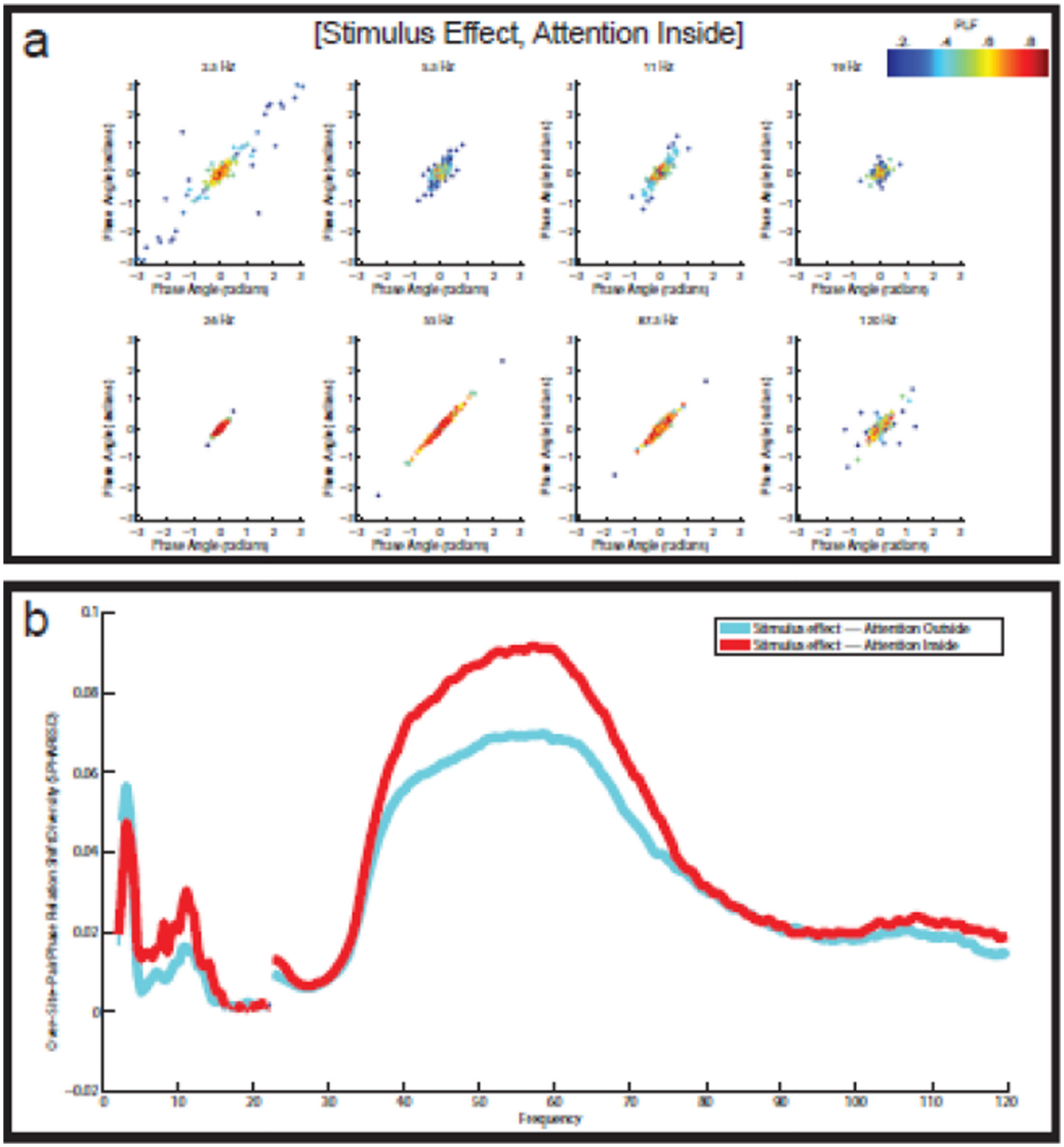

Figure 6. Reliable diversity in the stimulus-induced LFP-LFP phase relation shifts

(a) Split-half scatter plots of the stimulus-induced LFP-LFP phase relation shifts for eight different frequencies in the attention inside condition. The points in the scatter plots are color-coded according to the PLF of the corresponding channel pair. There are reliable stimulus-induced phase relation shifts at 2.5 Hz, 11 Hz, and 55 Hz. Especially at 55 Hz, the phase relation shifts can be large, ranging from −1.2 to +1.2 radians. (b) SPHARESD spectra for the attention inside and the attention outside condition. The SPHARESD coefficients measure the reliable diversity in the stimulus-induced LFP-LFP phase relation shifts. In both attention conditions, there is reliable diversity in the stimulus-induced LFP-LFP phase relation shifts, and this in the same three frequency bands that also show reliable

LFP-LFP phase relations: low theta (3–4 Hz), alpha (9–13 Hz), and gamma (35–75 Hz). Statistical significance (with FDR-correction) is indicated by the thickness of the lines.

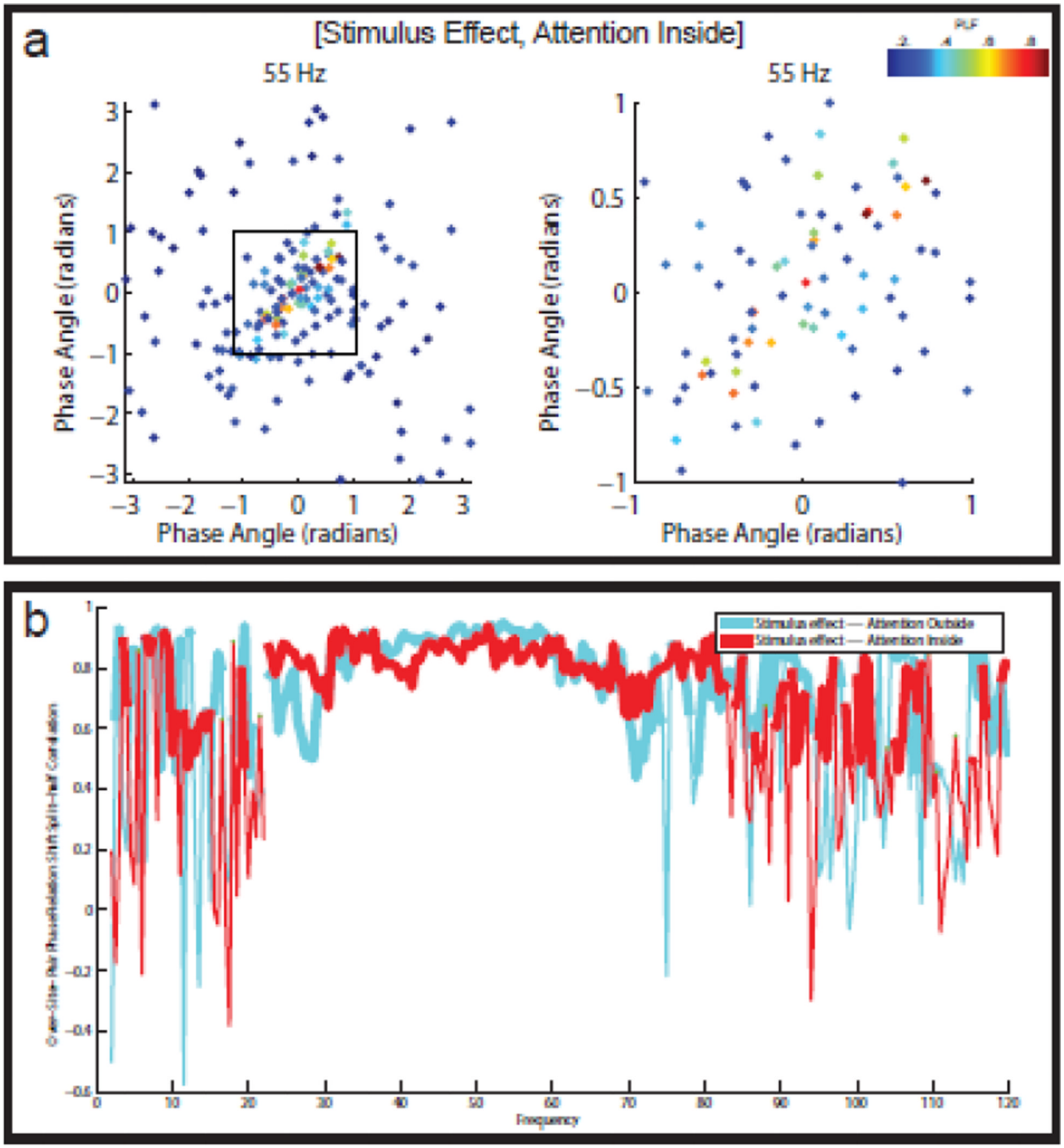

Figure 7. Reliable diversity in the stimulus-induced LFP-MUA phase relation shifts, but only for the channel pairs with a high consistency in LFP-MUA phase relation shifts

(a) Split-half scatter plot of the stimulus-induced LFP-MUA phase relation shifts at 55 Hz in the attention inside condition, with color-coding according to the PLF of the corresponding channel pair. The left panel shows the scatter plot using all LFP-MUA channel pairs, and the right panel shows only the center of this scatter plot (indicated by the square), which contains the channel pairs with the highest consistency in the LFP-MUA phase relation shifts. The 17 most reddish dots were used for calculating the split-half correlation. (b) Split-half correlation spectra for the attention inside and the attention outside condition. The split-half correlations were calculated on the 10 percent LFP-MUA channel pairs with the highest

consistency in the LFP-MUA phase relation shifts. For many frequencies, these split-half correlations indicate a reliable diversity in the stimulus-induced LFP-MUA phase relation shifts. This was most clear for the frequencies between 20 Hz and 80 Hz.

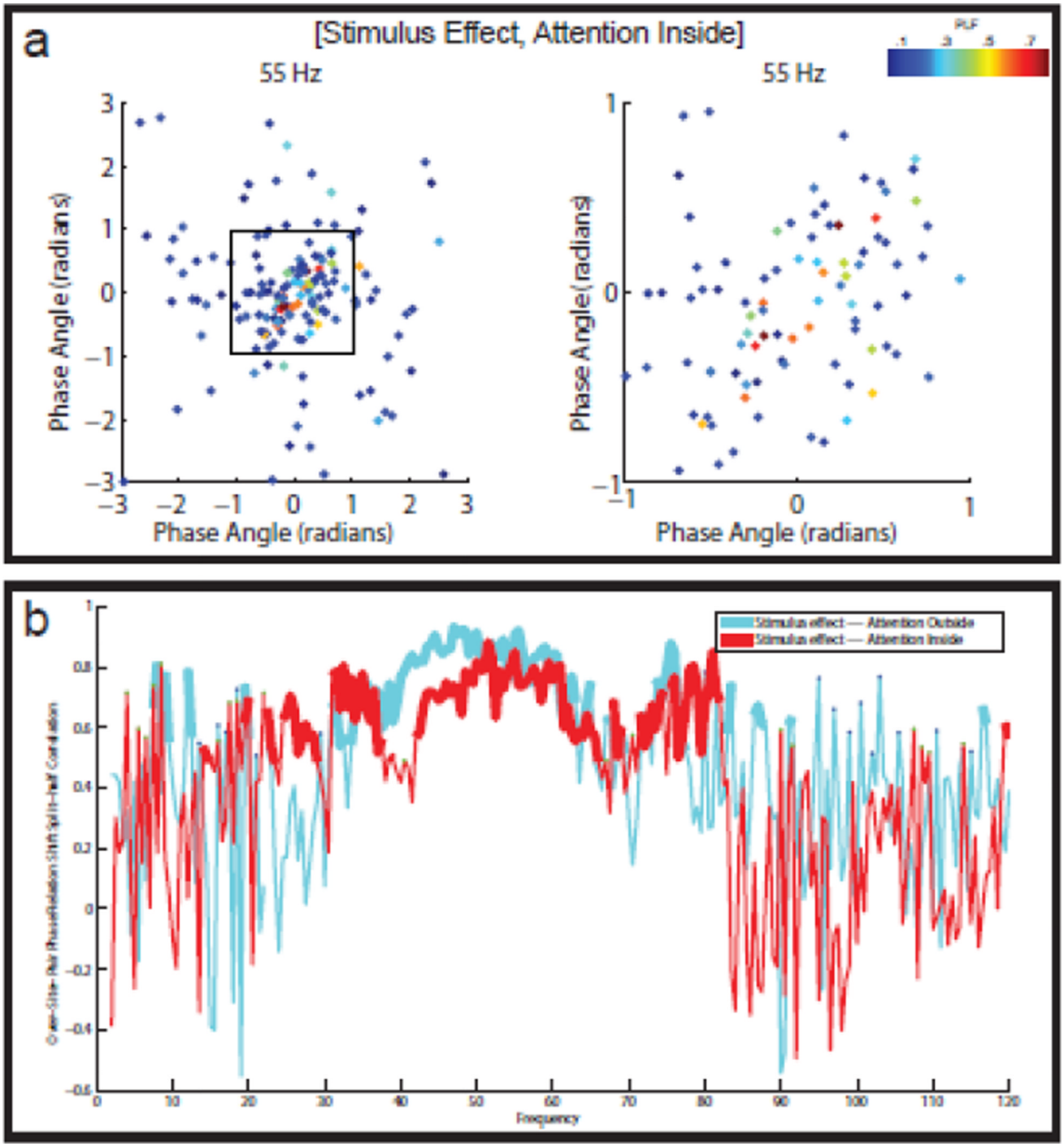

Figure 8. Reliable diversity in the LFP-centered stimulus-induced LFP-MUA phase relation shifts, but only for the channel pairs with a high consistency in LFP-MUA phase relation shifts

See the caption of Figure 6. The main difference with Figure 6 is that the stimulus-induced LFP-MUA phase relation shifts are now centered in an LFP-channel-specific way: stimulus-induced phase relation shifts were shifted by the average stimulus-induced phase relation shift calculated over the three LFP-MUA channel pairs that involve the same LFP channel (see Materials and Methods). Predominantly for the gamma (35–75 Hz) band, these split-half correlations indicate a reliable diversity in the LFP-centered stimulus-induced LFP-MUA phase relation shifts. Statistical significance (with FDR-correction) is indicated by the thickness of the lines.

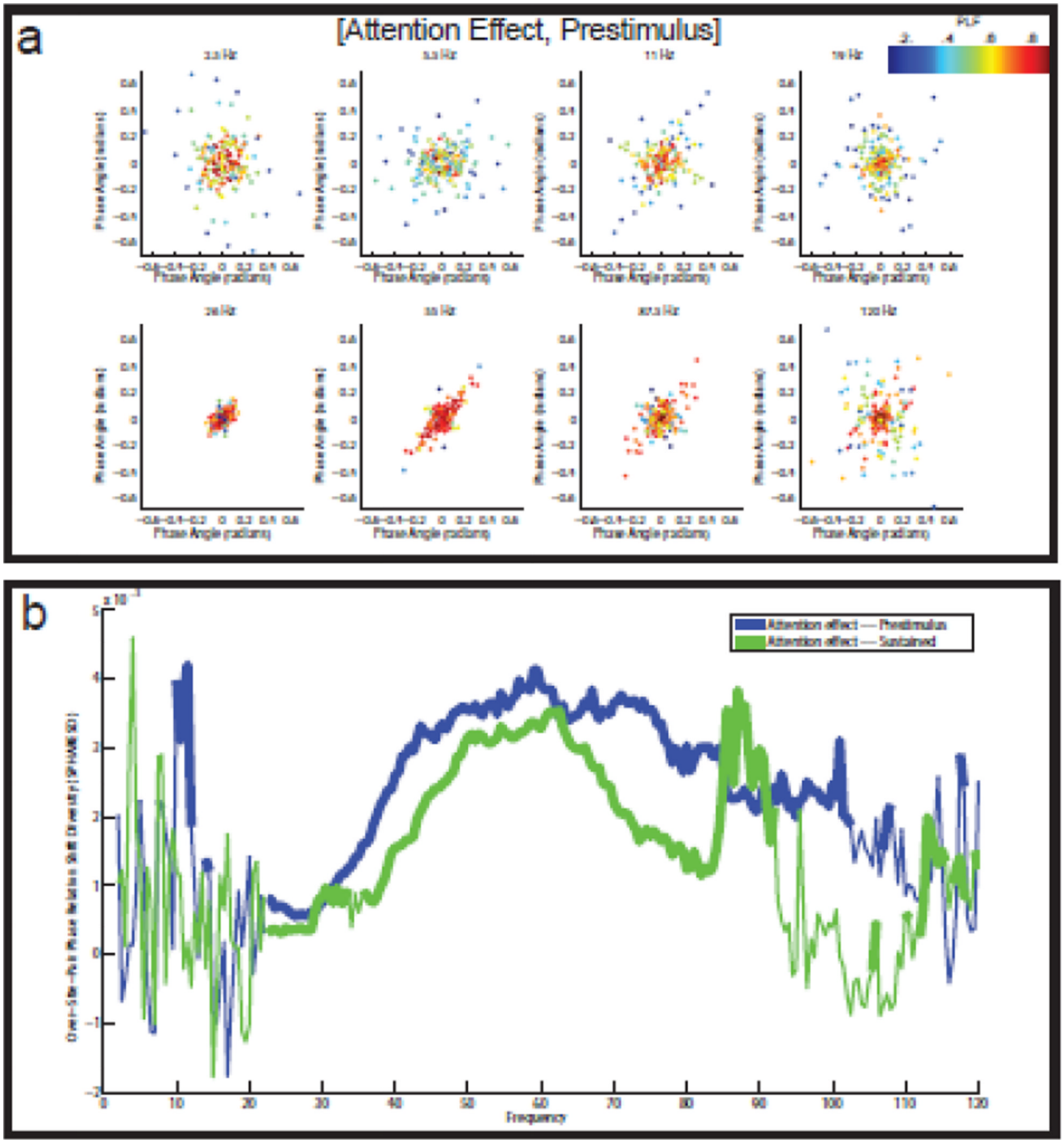

Figure 9. Reliable attention-induced LFP-LFP phase relation shifts

(a) Split-half scatter plots of the attention-induced LFP-LFP phase relation shifts for eight different frequencies in the pre-stimulus period. The points in the scatter plots are color-coded according to the PLF of the corresponding channel pair. There are reliable attention-induced phase shifts at 55 Hz. (b) SPHARESD spectra for the pre-stimulus and the sustained stimulation period. The SPHARESD coefficients measure the reliable diversity in the attention-induced LFP-LFP phase relation shifts. Statistical significance (with FDR-correction) is indicated by the thickness of the lines.